The Effect of Sand on the Wear of Anodized Aluminum

by

Sara Pope

A thesis submitted to the Graduate Faculty of
Auburn University
in partial fulfillment of the
requirements for the Degree of
Master of Science

Auburn, Alabama
December 13, 2014

Keywords: Wear, Abrasion, Sand

Approved by

Robert Jackson, Chair, Associate Professor of Mechanical Engineering
David Beale, Professor of Mechanical Engineering
Dan Marghitu, Professor of Mechanical Engineering

Abstract

Sand can cause excessive wear in mechanical systems, especially when the motion is frequent and small in amplitude. A modified block-on-flat wear test of anodized aluminum on hard coat anodized aluminum was used to study this effect. The experiments were performed with and without sand in order to study the effects of the sand. Two methods of adding sand were used. Profilometry was utilized to study the differences between the two methods. The sand appears to change the wear mechanism from an adhesive to an abrasive mechanism. Black wear particles formed both when there was sand and when there was not sand. The source of these particles has been investigated.

Wear rates have been calculated based on both the change in the masses of the samples and the change in the height of the blocks over the course of each test. The wear rates from the change in the masses are repeatable with and without sand, but the results for the change in height show no repeatability without sand. In addition, only in the presence of sand do the trends for the two methods agree. The wear rate was found to be non-linear as a function of load and therefore not in agreement with Archard's Wear Law. The wear rate also increased significantly when sand was present in the contact for the duration of the test.

Acknowledgments

I would like to start by thanking my advisor, Dr. Jackson, and the rest of my committee, Dr. Beale and Dr. Marghitu, for their guidance and support throughout this project.

Many thanks go to Dr. David King from the Department of Geology and Geography for his assistance in characterizing the problem sand.

I would also like to thank Mr. Hamid Ghaednia for his assistance with developing the image processing code for the experimental sand, as well as his unwavering support and willingness to listen to me talk about my work and practice presentations on him.

Special thanks go to my friends and fellow students in the tribology lab: Hamed Ghaednia, Xianzhang Wang, Yang Xu, Xiaohan Zhang, and Yang Zhou. I could not have wished for a better group of people to work and laugh with.

Finally, I have to thank my mother and my aunt, who have graciously supported me, listened to me explain my research far too many times, and encouraged me when I was sure I would fail. I cannot properly express my appreciation for everything they have done for me in words.

Table of Contents

List of Figures

List of Tables

Chapter 1

Introduction

Wear is an important product of surface interaction. The phenomenon of wear is present in many aspects of everyday life. Automobile parts like tires and windshield wiper blades have to be replaced periodically when wear removes enough of their material to render them not useful anymore. Any mechanical device experiences wear, from ATMs to industrial robotic arms, and any part that undergoes wear eventually has to be repaired or replaced, resulting in downtime for the machine while it is fixed. The parts, labor, and lost time can be very costly. Therefore, predicting and mitigating wear is very important.

Wear is the removal of a small amount of material from an object through mechanical action, often sliding. There are many types of wear. Adhesive wear occurs when two relatively smooth surfaces slide against each other and small fragments of each surface adhere to the other. These fragments can be transferred back and forth between the surfaces and may eventually break off to form wear particles. Abrasive wear comes in two forms. In two-body abrasion, a rough, hard surface scratches a softer surface as they slide against each other. In three-body abrasive wear, hard particles caught between two surfaces an cause wear through several mechanisms, including scratching and plowing. While adhesive and abrasive wear are the most common types of wear, there are other types, including corrosive wear, erosion, surface fatigue, and fretting wear. The small oscillatory motion associated with fretting wear can also amplify the effects of abrasive and adhesive wear.

Wear can be measured in several ways. Wear samples can be weighed before and after the test and the change in mass recorded. The wear grooves can be measured using a profilometer. The volume lost or moved from the groove can be calculated. This is especially useful if there is an area of particular interest on the component being studied. Very small

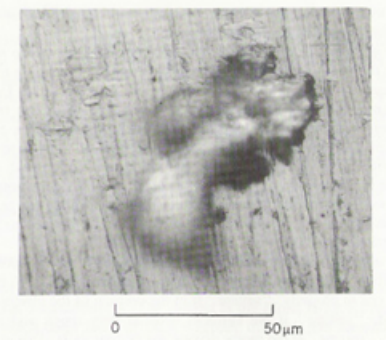

Figure 1.1: Adhesive wear particle [32]

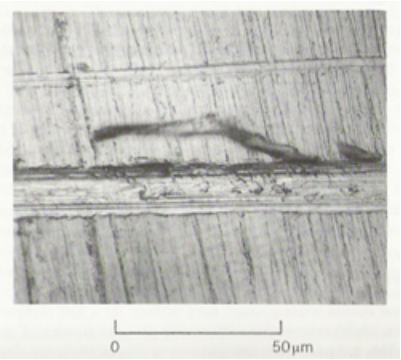

Figure 1.2: Abrasive wear scratch [32]

amounts of wear can be measured using radioactive tracers. The weighing method was used in this study, since the amount of wear on the entire component was large enough to measure with an analytical scale.

Aluminum is a strong, light metal, but it does not have the high hardness of steels. The anodic layer created by the anodization process on the surface of an aluminum or aluminum alloy part increases the hardness and corrosion resistance of that surface. It can also be dyed and sealed in a number of ways, both for aesthetic and practical purposes. These characteristics make anodized aluminum suitable for many applications in aircraft components, automobile parts, industrial equipment, personal electronics, and many others.

Many of these applications may be in sandy environments. Parts that may undergo little wear during normal use can experience wear an order of magnitude greater in sandy

environments, as shown in the current work. A system optimized for a clean environment may not be very resistant to abrasive wear. Therefore it is important to use laboratory wear tests to gain an understanding of how the intruding sand will affect the wear on these parts.

The purpose of this work has been to use a wear test to determine the effect of sand on the wear rates of materials typically used in a captive carry payload system on board a helicopter. Once a repeatable wear test has been established, it can be used to test any combination of materials or coatings. The wear rates obtained from these tests could also be used to predict the wear of other components in sandy environments.

1.1 Organization of Thesis

Chapter 2 is a background on wear, anodization, and various wear experiments. Both two and three body wear are covered.

Chapter 3 explains the experimental methodology, including materials used, the basics of sand, and the experimental setup.

Chapter 4 contains the results and discussion of all experiments performed.

Chapter 5 is a summary of the results and the conclusions. Future work is also laid out here.

Chapter 2

Literature Review

2.1 Introduction

Archard [2] studied wear and electrical contact resistance in the context of the models for contact between two surfaces. He found that the most realistic model for contacting surfaces is the one where discrete junctions exist between contacting asperities, which increase in both size and number as more load is applied. While using this model has a significant effect on the prediction of contact resistance, it has no effect on the prediction of wear. The equation he developed for two body adhesive wear was:

$$V = \frac{kPs}{H} \tag{2.1}$$

where V is the volume worn away, k is the dimensionless wear coefficient, P is the applied load, s is the sliding distance, and H is the hardness of the softer material. The dimensionless wear coefficient represents different quantities depending on the type of wear. In adhesion, k is $\frac{1}{3}$ the probability of a substantial wear particle forming. In abrasion, k is related geometrically to the surface features of the harder surface or abrading particles. The wear coefficient for two-body abrasion is typically an order of magnitude greater than that of three-body abrasion. The wear coefficient is constant for a set of materials. This can be rearranged to form:

$$\frac{V}{s} = \frac{kP}{H} \tag{2.2}$$

In the form of Equation 2.2, the left hand side is called the wear rate. Since k and H are assumed to be constant, this implies that the wear rate is directly proportional to

the applied load. Sliding velocity, temperature, and other environmental factors are not considered explicitly in this equation. Both equations are applicable to two body adhesive, two body abrasive, and three body abrasive wear.

Archard [3] also studied whether the Amontons friction law is consistent with the hypothesis that asperities deform elastically. The friction force should be proportional to the real area of contact as well as load, but for elastic contact, the applied load is not proportional to the real area of contact. The exponent on the applied load ranges from two-thirds at elastic contact to one for fully plastic contact. Archard determined that the Amontons law holds when plastic flow occurs at the contacts or when there are a large number of elastically deforming contact areas in series or of different sizes.

Abrasive wear can only occur when the abrasive particles are in contact with the sliding surfaces. With smaller particles, it becomes less likely that the surfaces are in contact with a specific particle. Williamson et al. [41] examined the probability of a surface contaminated with small particles coming into contact with another surface. This probability is related to the number and size of dust particles, the load applied, and the material properties of the surfaces.

2.1.1 Anodization

Aluminum is frequently used in applications where low weight and corrosion resistance are required. However, the high friction and wear rate of aluminum alloys typically limit the applications where they can be used. Anodizing is often used to improve these properties. Anodic coatings are porous, rather than solid [1]. The pores are conical, so the openings are larger at the surface. At a certain thickness, the pore openings will begin to intersect. This limiting thickness, as well as other parameters of the coating that result from the anodization process, can vary greatly depending on the electrolyte bath components, bath temperature, and anodizing current. MIL-A-8625F [26] specifies some of the anodizing parameters for several types of anodic coatings for specific applications, as well as the required qualities

of these coatings and test procedures for these qualities. The anodizing temperatures and currents depend on the alloy, so these are not specified. The two anodizing types used in the current work are Type II and Type III anodization.

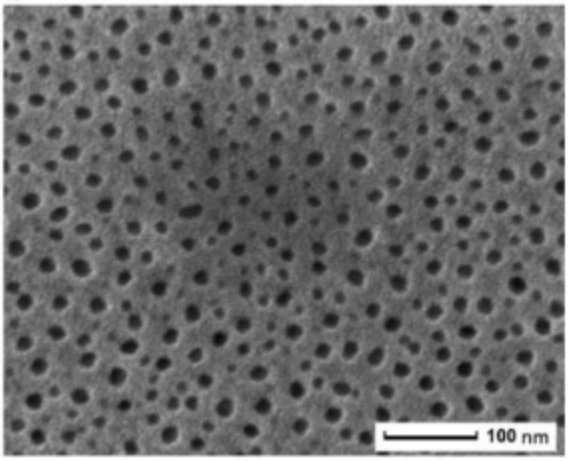

Figure 2.1: Porous structure of anodized aluminum [1]

Type II anodic coatings are created by treating aluminum or an aluminum alloy electrolytically in a bath containing sulfuric acid. These coatings can be sealed for additional corrosion resistance. The coating must weigh more than 1000 mg per square foot and be between 0.07 mil and 1 mil thick. Type III anodic coatings do not have to be created in a particular electrolyte bath. Any acid and process can be used, as long as it results in a heavy, dense coating of the desired thickness.

Type III coatings should not be applied to alloys made of more than 5% copper or 8% silicon. They also should not be coated unless there is a need for increased corrosion resistance, since sealing reduces the wear resistance of the coating. The Type III coatings have to be tested for abrasion resistance on a Taber abraser according to procedures in FED-STD-141C [16] with a 1000-gram load at 70 RPM for 10,000 cycles. The coating should not wear more than 3.5 mg per 1000 cycles for alloys containing more than 2% copper or more than 1.5 mg per 1000 cycles for any other alloys. The coating can be between 0.5 mil and 4.5 mil thick. For coatings less than 2 mils thick, the thickness cannot vary more than +/-

20%, and for coatings thicker than 2 mils, the thickness cannot vary by more than +/-0.4 mils.

Although anodizing does improve some properties of aluminum and its alloys, there may not be improvements in all loading conditions. Sadeler et.al. [34] looked at the effect of anodization on fretting fatigue. The small oscillatory motion of fretting reduces the fatigue life of aluminum parts. Hard coat anodizing can increase the fatigue life in fretting conditions at low stress levels but has little to no effect at higher stresses.

Emeric et al. [14] reported on the effect of different anodic coatings and surface treatments on aluminum alloys on fatigue strength. Since the oxide formed by anodization is brittle, anodizing typically reduces the fatigue strength of aluminum alloys. However, this effect can be mitigated by shot-peening the anodized surface if integral color anodizing or Type III anodizing was used.

2.1.2 Abrasive Particle Characterization

Abrasive particles are typically characterized by their size and angularity. Particle size can be controlled by sieving [6]. Angularity can be quantitatively measured [37] or given a qualitative description by comparing particles to standard models [30].

2.2 Two Body Wear

Archard and Hirst [4] studied the two body wear of many metal combinations in unlubricated conditions at numerous speeds and loads to investigate the claim that the wear rate is proportional to the load, assuming all other material properties are constant. They observed two forms of wear: mild wear at lower loads and severe wear at higher loads. Certain material combinations can vary between these two types of wear, since they are also affected by the surface conditions of the sliding materials. In a few of the many cases they studied, the load was proportional to the wear rate. However, they determined that for many cases, the relationship is close enough to being proportional that a linear relationship

can be assumed without too much error. This assumption allowed them to calculate wear coefficients for many material combinations.

Nuruzzaman and Chowdhury [28] examined the friction and wear of copper and aluminum against steel in a pin-on-disc test at three loads and three sliding velocities. The wear was measured by weighing. The copper and aluminum discs had approximately the same roughness. The friction coefficients of both decreased with increasing load and increased with increasing sliding speed. The wear rates of both materials increased with increasing sliding speed and load. For all cases, copper had a lower friction coefficient and wear rate.

Mehta et al. [24] looked at the wear properties of die- and sand-cast magnesium and aluminum alloys under dry and wet sliding conditions in pin-on-disk tests. They especially wanted to see if magnesium could be used in place of aluminum for automotive applications, since it is not as dense. However, the aluminum alloys had higher hardness and better wear properties in all cases, regardless of the casting method. They reported a linear relationship between wear rate and load, although they only used two loads in their tests.

Spuzic et al. [36] used the statistical method of fractional experiment design to study the effects of force, operating temperature, material, and sliding velocity on wear during a hot rolling process. The operating temperature affects the type of oxide that forms on the materials used. Some oxides are more prone to fracturing and removal, thus becoming abrasive particles that cause more wear. Increasing the sliding velocity actually decreases the abrasive wear at higher temperatures. Overall, the combinations of sliding velocity, material, and operating temperature had the most significant effects on the abrasive wear. The load had less of an effect.

2.3 Three Body Wear

Three body wear is a complicated phenomenon. The wear depends not only on the material properties of the sliding materials but also on the material, geometric, and size

properties of the abrasive particles. In some situations, large particles cannot enter a system, but small particles can cause a large amount of wear. In other cases, large particles cause much more damage than small particles. Material can be worn away through cutting, wedging, or fatigue caused by plastic deformation caused by rolling particles. Even the way the particles enter the system affects the overall wear. Additionally, obtaining repeatable results can be very difficult or nearly impossible for some experimental setups.

Bingley and Schnee attempted to develop a predictive model for three body abrasive wear [8]. They observed that three body wear typically has a lower wear rate than two-body abrasive wear. They assumed that this was due to the ability of the loose particles to roll, rather than always sliding and plowing through the surfaces. Their equations are based on the assumption that rolling angular particles indent and plastically deform the surfaces, eventually removing material through fatigue. This also means that the particle size has an effect on the wear rate. They tested their predictions in dry and lubricated tests on a lapping and polishing apparatus. This wear model worked best for lubricated conditions with small particles. In the other cases, sliding was the dominant particle motion, especially with larger particles. They also saw that the load has a greater effect than the abrasive particle size, especially in dry conditions.

Tonghai et al. [38] studied the abrasive wear mechanisms in automated teller machine (ATM) roller-scraper systems in sand-dust environments. As wear progresses in the system, the diameter of particles entering and the wear mechanism changes. The mildest form is microcutting caused by tiny particles. As the wear grooves grow, larger particles can enter the contact area and plow deeper grooves. The deeper grooves allow even larger particles to enter and remove chips of the material through wedging.

Stachowiak and Stachowiak [37] looked at the effect of abrasive grain shape and material on three-body wear. They quantified the angularity of the particles using the spike parameter-quadratic fit (SPQ), which looks at the corners outside the average radius of the

grains that are most likely to come into contact with the sliding bodies. The best correlation came from the ball-on-plate abrasive slurry tests. The wear generally increased with increasing angularity, with the exception of the quartz abrasive. The quartz grains were more oblong than spherical, so they tended to become oriented in a way that most of the edges were out of contact.

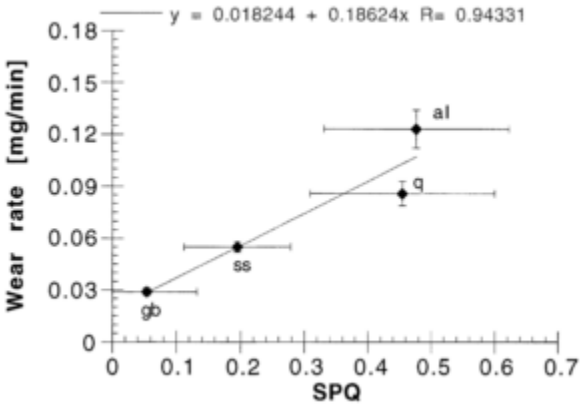

Figure 2.2: Wear rate versus quantitative angularity [37]

Siebert [35] conducted the ground tests for the Mars rover Sojourner Wheel Abrasion Experiment (WAE). The palagonite grains (median diameter of 6000 μm) caused the most wear and scratches, despite being less angular than the other two. The Minnesota lunar simulant (median diameter of 5 μm) caused the least overall wear but did wear and polish all sets of samples. The Arizona lunar simulant (median diameter of 50 μm) caused some polishing but there were also scratches. Some dust did stick to the wear strips, so the photocell outputs have to calibrated to accurately measure the wear, since there would be no way to clean the dust off of the Mars rover during the Pathfinder mission.

Ferguson et al. [17] worked on the WAE that was aboard the Mars rover Sojourner. Strips of aluminum, nickel, and platinum of several thicknesses were deposited on top of a panel of black anodized aluminum on one of the rover's wheels. These materials were chosen as representatives for structural, electronic, and propulsion applications, respectively. The wear of the strips was determined by the percent of light that reflected off of the strips after

rolling through the Martian soil. The ground tests performed by Siebert [35] with three types of soil simulants were used to better determine the characteristics of the Martian soil. The aluminum samples on the rover were polished, but those in the ground test were not. From this, they were able to estimate that the average particle size of Martian soil is 10 – 20 μm. Additionally, only the aluminum and platinum were abraded; the nickel showed no signs of abrasion. Therefore, the soil had to have a hardness greater than or equal that of platinum but less than that of nickel. Wear tests can provide valuable information about environments just by comparing them to a similar test in a known environment.

Fernández et al. [18] studied the effects of high and low levels of applied load, particle reinforcement of the nickel coating, and abrasive grain size, as well as wet and dry environments. Both sizes of the Al_2O_3 abrasive had similar angularity to eliminate the effects of particle geometry. Wear was measured by weighing to the nearest 0.1 mg. A series of sixteen tests was run in order to compare the effects of each variable. They found that the abrasive grain size and the coating reinforcement had a much greater effect than the applied load. There was only a small difference in wear between the wet and dry environments.

Li and Yan [22] tested polymers on a block-on-ring tribometer in still air, blowing air, and blowing sand environments. Typical tests with sand feed grains into the contact, which is much more severe than a typical application. Since the purpose of the study was to compare wear in different environments, a realistic blowing sand environment was developed. The blowing air and blowing sand environments improved the wear behavior of two of the polymers, but the third performed better in the still air.

Quercia et al. [31] looked at the friction and wear behavior of several hard materials as possible replacements for typical steel parts in the oil industry. The abrasion tests were carried out on a ball-cratering microabrasion apparatus with diamond-lapping paste. For all but the highest tested load (10 N), the steel performed better than the other materials in the friction tests. All tested materials showed a linear relationship between abrasive wear volume and sliding distance times the applied force.

Kumar et al. [21] tested six aluminum alloys on a dry sand rubber wheel apparatus. Angular SiO_2 particles with a diameter of 150-250 μm and loads from 5-20 N were used. Wear was measured by weighing every five minutes, and the tests were run until the wear rate reached a constant value. The wear rate decreased from the beginning of the test until steady-state wear behavior was reached at a sliding distance of approximately 5760 m. The wear rate increased with increasing load, regardless of the alloy, but the heat-treated alloys wore less, presumably because they have higher hardnesses.

Trezona and Hutchings [39] used a ball-cratering micro-scale abrasion apparatus to study the three body wear of PMMA, aluminum, tool steel, and glass-bonded alumina. The most repeatable results occurred when a hard, rough ball was used at low loads with a high abrasive slurry concentration. The rough ball allowed particles to enter the contact area more easily. At lower loads, there are more gaps between the surfaces due to the roughness of the ball, allowing more particles to become entrained in those gaps. With a lower load and more particles in the contact area, the load is less concentrated on each particle.

Du et al. [13] looked at the effect of reinforcing nickel coatings with various nano-particles on the wear of components sliding in a lubricant contaminated with abrasive particles. Fine sand particles accelerate wear in lubricated sliding components, which is a problem in dusty environments. Al_2O_3 and SiO_2 abrasive particles were sieved to remove particles with a diameter greater than 50 μm and mixed with a diesel oil lubricant. A ball-on-disk tribometer was used. The wear was too small to be measured by weighing, so the wear volume was calculated from measurements made under an optical microscope. Only two of the nano-particles reduced the friction and wear of the nickel coating. These nano-particles reduced the size of the nickel grains that formed in the coating, which made the coating harder and more compactly structured.

The wear caused by abrasive particles can severely affect the performance of the worn parts. Gao et al. [19] studied the effect of particulate contamination on the fretting failure of electrical connectors. Quartz sand with diameters ranging from 1-30 μm were sprayed

onto an electrical connector surface before being subjected to a vibration test. The particles increased the fretting and abrasion of the connector parts, as well as increasing the contact resistance. A FEM simulation was also developed to evaluate the vibration thresholds for both contaminated and uncontaminated connector sets. The sand contamination decreased the fretting threshold while increased the amplitude and frequency of the first resonant peak.

2.4 Wear on Anodized Aluminum

Aerts et al. [1] analyzed the effect of the anodizing electrolyte temperature on the microhardness and fretting wear resistance of the resulting anodization on commercially pure aluminum. They tested coatings created in the range of 5 °C to 55 °C, as well as analyzed the coatings microstructure. They found that the size of the pores created during the anodization process was directly related to the microhardness, but it was only one factor of many in the fretting wear resistance of the anodization.

Bensalah et al. [7] included various concentrations of oxalic acid in the typical sulphuric acid electrolyte and tested the resulting anodic coatings for Vickers microhardness and abrasion resistance. Adding oxalic acid increased both the abrasion resistance and the hardness of the coatings. This effect was especially prominent when used in conjunction with the optimal electrolyte temperature and current density during the anodization process.

Chou and Leidheiser [11] studied the abrasive wear process of two flat panels of anodized aluminum sliding back and forth against each other in an abrasive slurry consisting of silicon carbide abrasive particles (average diameter about 1 μm) dispersed in distilled water. They varied the concentration of SiC particles in the slurry and the anodization thickness to see the effects on the wear. The dominant wear mechanisms were cutting and plowing. At low concentrations of SiC, increasing the concentration greatly increased wear, but after a certain point, the wear leveled off with respect to slurry concentration. They also noted that the wear rate increased with increasing coating thickness, likely due to the porous structure

of the anodization. Therefore, the anodization process has a significant effect on the wear properties and hardness of the final coating.

The anodization process does have a large impact on the resulting coating, but the fabrication of the aluminum part also affects the formation of the coating. Riddar et al. [33] studied the effect of the fabrication method on the final anodized surface of aluminum cylinders used in clutch actuators. The cylinders were produced by permanent mold casting, sand casting, extrusion, and high pressure die casting. The surface topography of the un-anodized and anodized cylinders, nanohardness, and abrasive wear characteristics of the anodized cylinders were studied. The roughnesses of the cast surfaces were around 0.2 – 0.3 μm, while the extruded cylinder had a lower roughness. The anodizing increased the roughness of the cylinders. The extruded cylinder had the thickest anodization of the four. The extruded cylinder also had the highest wear rate and average nanohardness. The fabrication method used depends on the application and desired performance of the material.

The methods used to clean and treat the surfaces before anodizing can also affect the properties of the final anodic coating. Markowitz [23] studied the effect of coating thickness, pre-anodizing cleaning method, and compressive stress treatments on the quality of hard coat anodic coatings on 7075-T6 aluminum. Specimens were tested on the Taber abraser and the resulting wear evaluated visually. Anodic coatings are porous by nature. As the coating gets thicker, the pores grow larger, and voids can form under the surface of the coating. These voids reduce the abrasion resistance of the anodization. Most of the cleaning methods did not affect the abrasion resistance, but etching did produce a significantly lower wear resistance. The compressive stress treatments tested did not adversely affect the abrasive wear resistance of the anodized aluminum alloy.

In some applications, anodic coatings may be treated for additional corrosion resistance or sealing. These processes may have adverse effects on wear though. Campbell et al. [9] tested the effect of additional topcoats on anodized aluminum and magnesium alloys. Magnesium alloys are desirable materials because of their lower densities; however, they are

susceptible to corrosion. Anodization mitigates this effect, but the protection provided by the anodic layer is reduced as it wears away. The topcoats were tested to see if they provided additional wear resistance. Wear was measured by weight after a Taber abraser test. For both the aluminum alloy and the magnesium alloy, the topcoat did not improve the wear resistance by much. The anodization had a much greater effect. The anodic layer on the aluminum wore less than the layer on the magnesium.

Westre et al. and Cheng and Hao [10, 40] tested the wear resistance and hardness of Type III anodized aluminum post-treated with various sealing and dyeing processes. It is generally assumed that any dyeing or sealing on a Type III coating will reduce both its wear resistance and hardness. The Taber abraser test was used to study the wear, since there are guidelines in MIL-A-8625 [26] and FED-STD-141C [16] for acceptable weight loss for a Type III coating. All of the dyeing and sealing processes increased the amount of wear on the anodized aluminum, but a few still stayed within the tolerances of the Type III testing. The Vickers hardness was measured three times on a coupon of each dyeing or sealing process, as well as an original untreated Type III coupon. None of the post-treatment processes increased or decreased the hardness of the anodization.

Noble and Leidheiser [27] were interested in the abrasive wear on anodized aluminum-polymer lithographic plates. When the surface of a lithographic plate is worn, the image quality decreases. An accelerated wear test in an aqueous solution typically seen in the printing process was developed. Pitting of the anodization was caused by fracture of the oxide coating, especially where the polymers did not cover the anodized aluminum.

Both Chou and Leidheiser [11] and Markowitz [23] observed that the wear rate of anodic coatings increase with increasing thickness and that this effect is caused by the porous nature of the coating. This effects the coating thickness that should be chosen in certain applications. For an anodized part, if the dimensions need to stay within a tight tolerance, a thinner layer is the better choice. The material will wear away more slowly and remain closer to the original dimensions. However, if the dimensions have a looser tolerance, a

thicker layer can be used. There is more material to wear away in a thicker anodic coating, so even though the wear rate is higher, the coating will last longer.

Chapter 3

Experimental Methodology

3.1 Wear Materials

Two sets of samples were used in the experiments. Both sets were made of aluminum alloy 7075-T651, and the composition is shown in Table 3.1. The T651 tempering means the alloy is solution heat treated, stress-relieved by stretching, and artificially aged [25]. This treatment leads to a higher yield strength than the original alloy. The upper samples (Figure 3.2) were anodized as specified in MIL-A-8625F for Type II Class 1 [26]. The lower samples were cut from components that are Type III hard coat anodized [26].

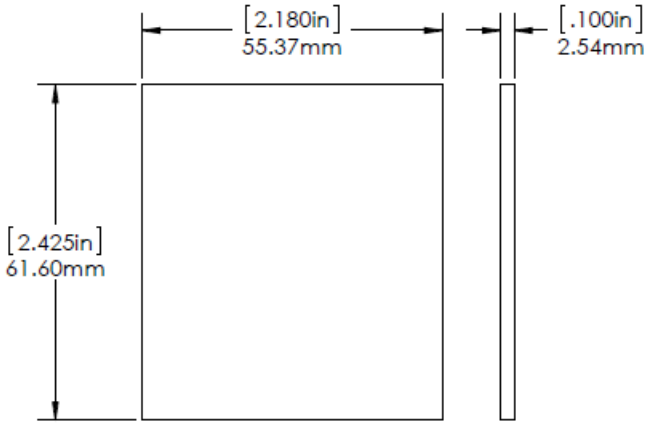

Figure 3.1: Draft of lower sample

3.2 Sand

The abrasive particles used in this study are generally referred to as sand. However, sand is one classification of the broad material of soil [6]. Soil can be formed in situ as either weathered rock or partially decomposed plant materials, or it can be transported by glaciers,

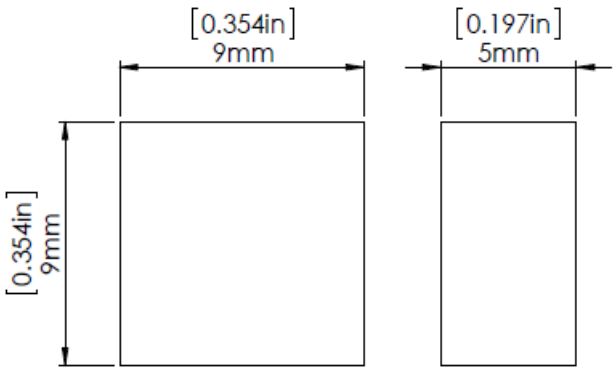

Figure 3.2: Draft of upper sample

Element	Weight Percent
Al	87.1-91.4
Zn	5.1-6.1
Mg	2.1-2.9
Cu	1.2-2.0
Fe	<0.5
Si	<0.4
Mn	<0.3
Ti	<0.2
Cr	0.18-0.28

Table 3.1: Composition of aluminum alloy 7075 [25]

water, or wind. Soils carried by ocean waters are referred to as oceanic, while soils carried by wind are called aeolian.

Any type of soil can contain different types of particles. The particles used here are mainly composed of hard granular particles made of hard rock minerals. Soil can also contain plant residues, clay minerals, and soft granular particles, like coral, shell, and volcanic ash. The size of these particles affects the overall classification of the soil. The size ranges for these classifications are shown in Table 3.2. The particles are also classified by their sphericity and angularity. Previously, measurements of the radii of the edges had to be made to determine the angularity. This method was not well suited to characterizing large amounts of particles in a short amount of time, and the values associated with specific angularities were not

Particle Type	Grain Diameter
Clay	<0.002 μm
Fine Silt	2-6.3 μm
Medium Silt	6.3-20 μm
Coarse Silt	20-63 μm
Fine Sand	63-200 μm
Medium Sand	200-630 μm
Coarse Sand	0.63-2 mm

Table 3.2: Soil particle sizing [6]

standardized. The most commonly used measure for these qualities now comes from the comparative models Powers created [30], shown in Figure 3.3.

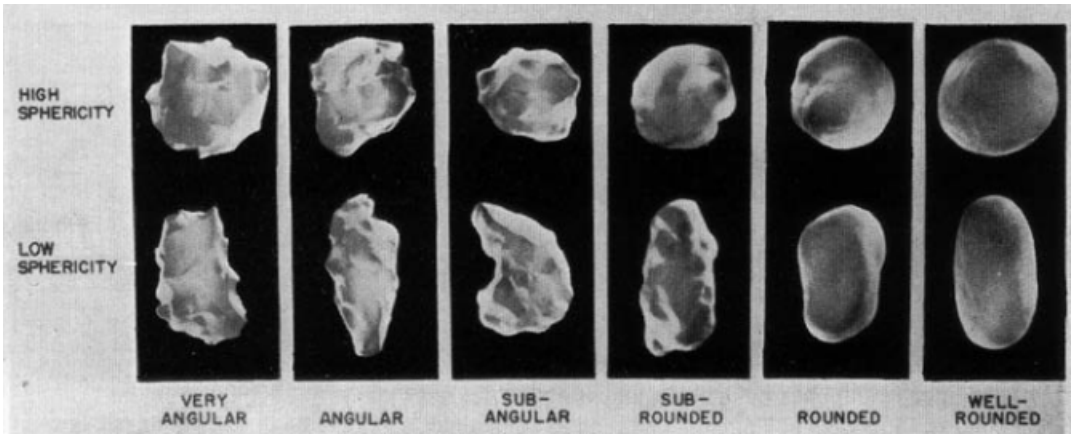

Figure 3.3: Soil grain angularity [30]

3.2.1 Foreign Sand

A small amount of the soil from the problem region was examined by Dr. David King of the Geology and Geography Department, as shown in Figure 3.4. He determined that the majority of the particles were quartz and feldspar. The full mineralogy can be found in Figure 3.5. The quartz and feldspar ranged in size from 10 μm up to 250 μm, making the soil a fine to medium sand. The other grains averaged around 135 μm. The quartz and feldspar were angular to slightly subangular, while the rest of the grains were mainly rounded to subrounded. Although many elements of the sand indicate that it is of aeolian

origin, the quartz and felspar are too angular. Since this sand was scraped off of components that have returned from the problem region, it is likely that the grains were crushed and that the sample is biased.

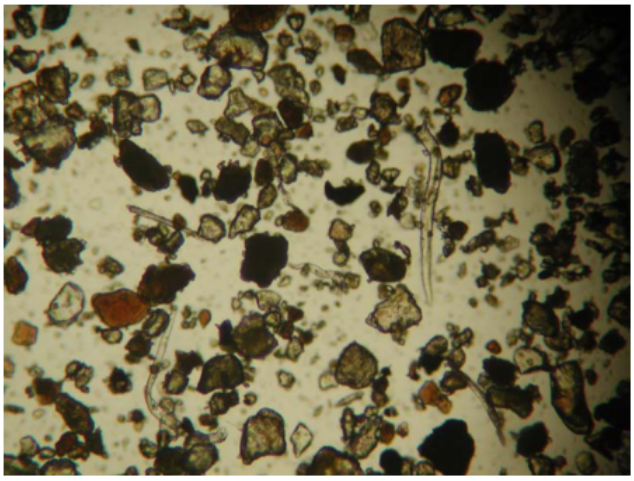

Figure 3.4: Foreign sand

3.2.2 Surrogate Sand

Since the supply of problem sand was limited, a surrogate sand had to be used. The most important factors were grain size and grain angularity. The most promising possibility was a refined, crushed silica sand from US Silica. The maximum grain diameter was 250 microns, similar to the problem sand. It is also angular. However, crushing silica creates silica dust (particles less than 10 microns in diameter), which is a health hazard and causes lung cancer with extended exposure. Sand used in PGA golf courses is also very standardized, but the average grain diameter is 1 mm, far larger than the problem sand [29]. Beach sand is more rounded, but in some places the sand is close to 250 microns.

Sand from Clearwater Beach, FL was collected and analyzed. The grains are mostly sub-angular to sub-rounded quartz. An image processing script was developed in MATLAB^{TM} to find the distribution of the grain diameters. Grains were spread out on a black background and photographed under a microscope. Care was taken so that no grain was photographed

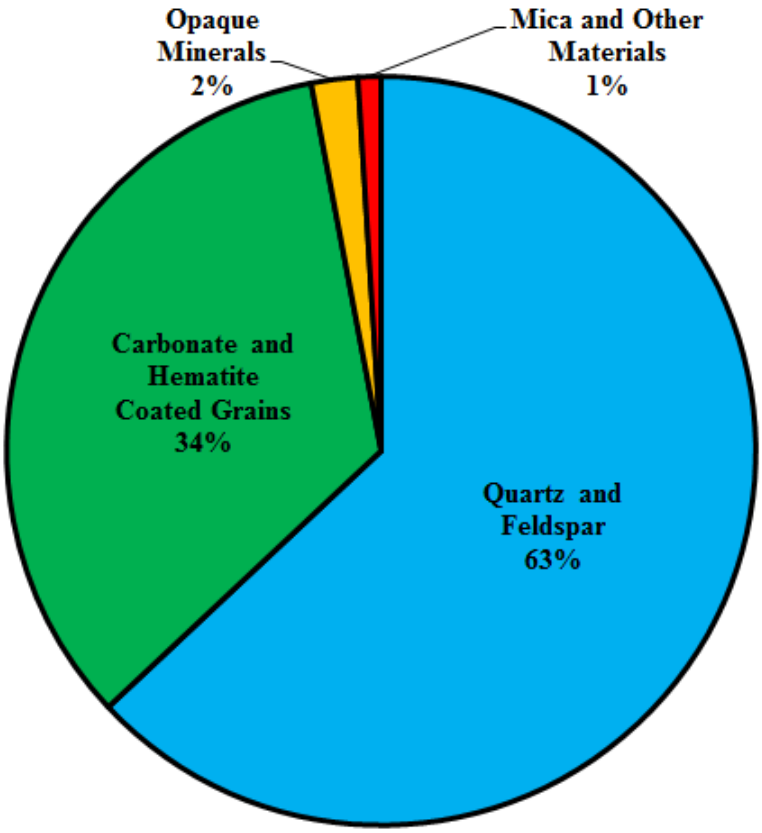

Figure 3.5: Composition of foreign sand

twice. A scale was photographed after every 6 grain photographs and used to define 1 mm in terms of pixels for that set of images. Once the scale was set within the script, the accompanying images could be analyzed.

First, the original image is imported into MATLAB^{TM} (Figure 3.6). Although the image appears to be in black and white, the image information is stored in RBG. The image is converted into grayscale (Figure 3.7). In grayscale, each pixel is defined by a number between 1 and 256, with 1 being pure black and 256 being pure white. A threshold value is chosen to define which pixels are part of the grains and which pixels are part of the black background. Pixels with a value greater than the threshold value are converted to pure white, and the rest are converted to pure black (Figure 3.8). Once the pixels are assigned a black or white

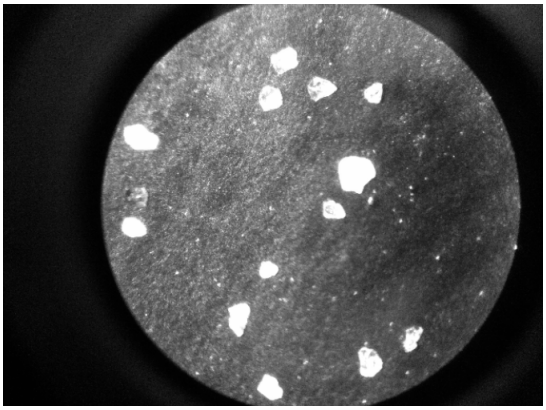

Figure 3.6: Original color image

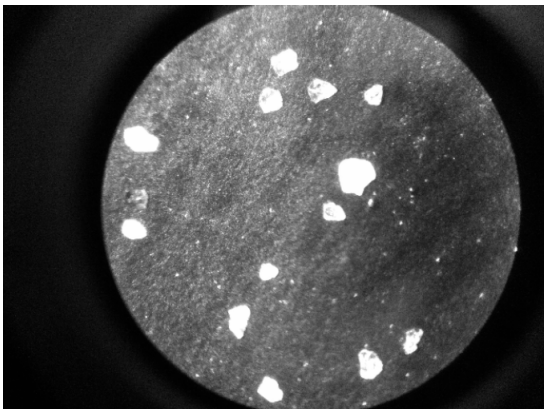

Figure 3.7: Image converted to grayscale

value, a built-in function is used to find the boundaries between black and white, which mark the grain boundaries. The center of each grain is then calculated by taking the average of the locations of each point on the grains boundary (Figure 3.9). The average radius of each grain is then calculated from the average distance between the center and its boundary pixels, illustrated in Figure 3.10. These average radii are doubled to get the average diameters, and these values are exported to a spreadsheet.

The results from 27 images were used to create the distribution of the grain diameters in Figure 3.11. The average diameter of the grains measured was 205 microns. Several grains were much larger than 250 microns. In order to bring the average grain size closer to the problem sand and to eliminate the larger grains, the sand was sieved using a 250-micron

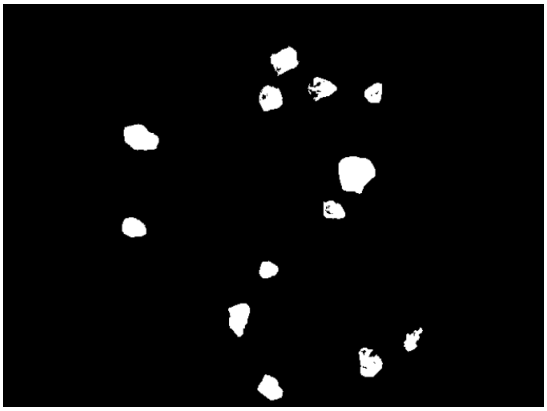

Figure 3.8: Grains after conversion to pure black and white

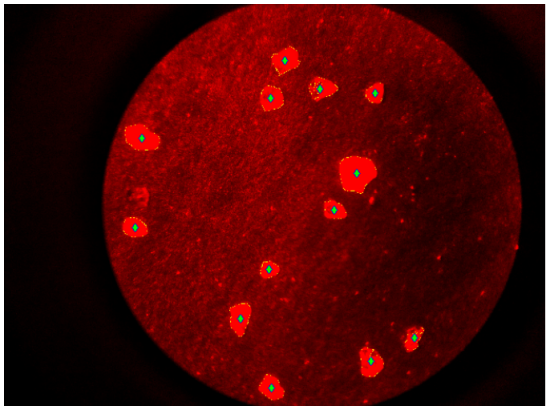

Figure 3.9: Plotted borders and centers of grains

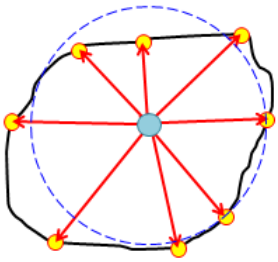

Figure 3.10: Schematic of radii calculation

opening sieve. The sieved sand was also photographed and the distribution of the grain diameters found. The average diameter was reduced to 190 microns. Most of the larger particles were eliminated as well as can be seen in Figure 3.12. Since the larger grains are more likely to have an effect on the wear than the average diameter, eliminating the larger

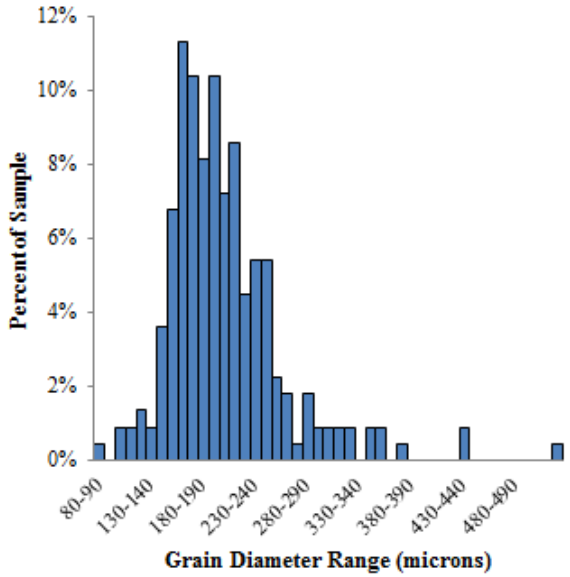

Figure 3.11: Sand grain distribution before sieving

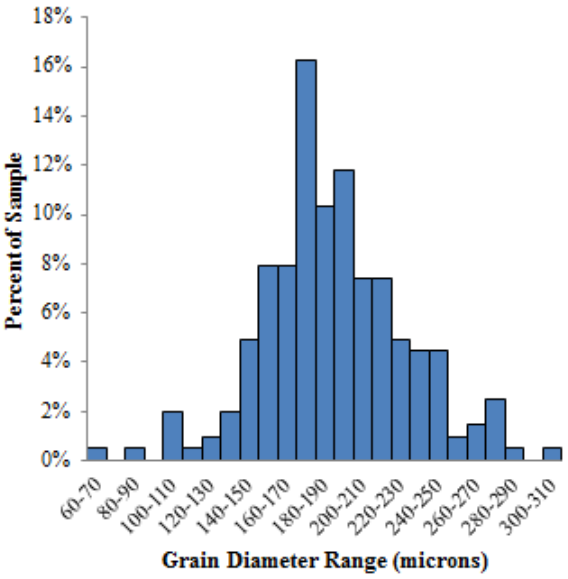

Figure 3.12: Sand grain distribution after sieving

particles is sufficient for the purposes of these tests. Additionally, having a more uniform sand should improve repeatability.

3.3 Experimental Setup

The tests were run on a CETR/Bruker UMT-3 Tribology tester with a rotary drive, torque sensor, and load sensor. The UMT can measure many quantities during a test. The quantities used from these tests were torque, applied load, height of the upper carriage, rotational velocity, and speed of the upper carriage.

Sensor	TH-50-0929	DFH-50-0911
Quantity Measured	Torque	Vertical Force
Maximum Value	12 N-m	500 N

Table 3.3: UMT modules

The bottom fixture had to be able to secure the lower sample during oscillation and contain sand with a low chance of it getting into the inside of the UMT. Additionally, the rotary platform is only a bit wider than the longest dimension of the lower samples, so the walls of the reservoir had to be fairly thin. The sample was held in place by four washers. Plastic spacers were used under the washers to keep them level. The bolt holes for the washers did not go all the way through the base so that the sand would be contained.

The upper fixture was designed to hold three samples spaced equidistantly at the same radius and parallel to the lower samples in three longitudinal rectangular grooves located 120° apart. A piece of metal was used as a spacer to ensure that the samples were aligned at the same radial distance. By changing the length of the spacers, the radial location or length of the samples could be adjusted. A screw at the outside end of the groove held the samples in place against the spacer. A rubber shim was placed between the base of the sample and the bottom of the groove to ensure that all three samples stay in contact throughout the test. Without the rubber shim, part of the samples would come out of contact during the test and would not wear, as in Figure 3.15.

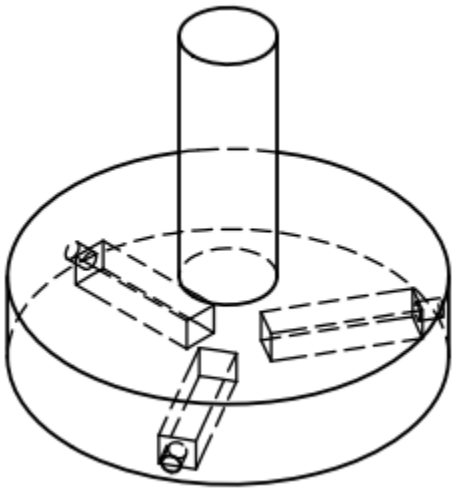

Figure 3.13: Schematic of upper fixture

Figure 3.14: Lower fixture

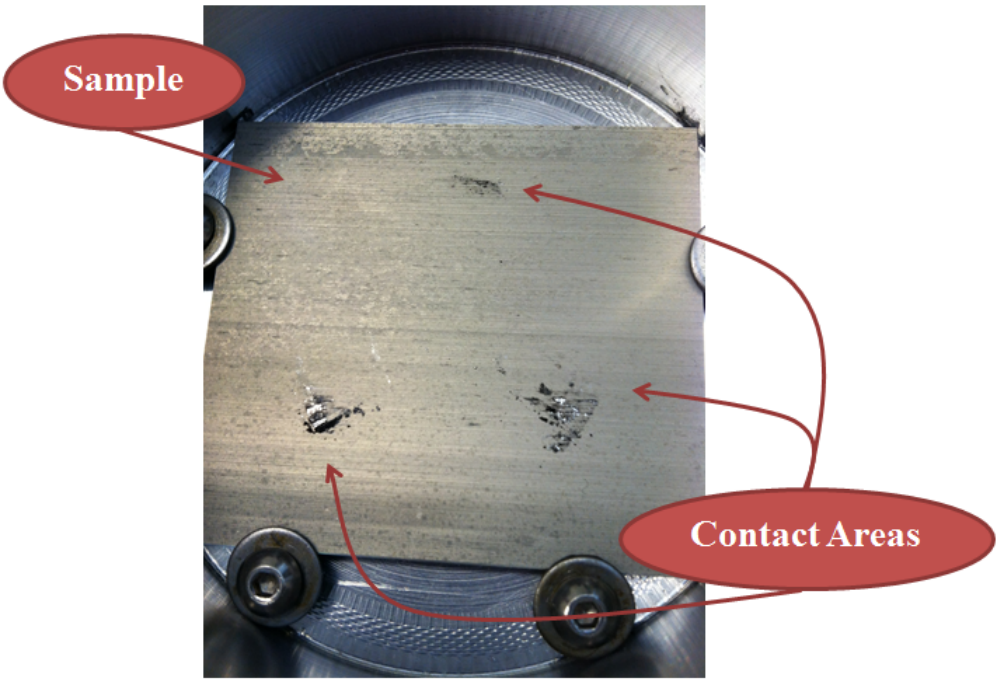

Figure 3.15: Sample after test without rubber shim

3.4 Test Details

The samples used were 7075-T651 anodized aluminum. The lower samples (2.175" x 2.425" x 0.125") were cut from existing components with Type III anodizing. The upper samples (9 mm x 5 mm x 9 mm) were cut from three-foot-long bars of Type II anodized 7075-T651. All samples were weighed before and after each test on an analytical scale that had a precision of 0.00001 g for items up to 30 g and 0.0001 g for items up to 120 g.

Thirty tests were run. Each test lasted 90 minutes. The bottom fixture rotated back and forth through 21.6° at 50 cycles/min. This rotation gives an average sliding distance of 2 mm per cycle on each sample, or a total of 9 m per groove. Five loads were used from 50 N - 250 N (0.37 MPa – 1.85 MPa). Tests at each load were performed with and without sand in 3 sets of 10 tests. The order of the tests in each set was chosen randomly. The order is shown in Table 3.4.

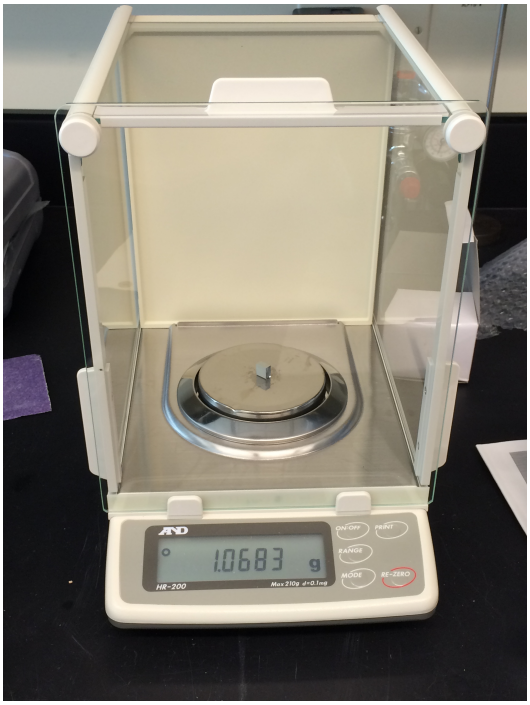

Figure 3.16: Analytical balance

The initial plan was to use loads from 200 N to 450 N in 50 N intervals, or 1.48 - 3.33 MPa. This was meant to match the range of pressures that could be felt by a captive carry payload system at rest and at the maximum acceleration, as specified in MIL-STD-810G Method 514.6 for an external store [12]. However, due to the oscillating test setup, the applied force for the UMT also varies. At loads greater than 400 N, the load swings high enough to trigger the automatic shutoff on the force sensor. To avoid this problem, the load range was reduced to 50 N - 250 N (0.37 MPa - 1.85 MPa). Since the vibration testing is

	No Sand			Sand		
Load	Round 1	Round 2	Round 3	Round 1	Round 2	Round 3
50 N	4	24	28	9	22	30
100 N	7	18	26	12	19	27
150 N	8	20	29	14	17	33
200 N	10	16	34	13	23	32
250 N	6	15	31	11	21	25

Table 3.4: Test matrix with sample numbers

supposed to be accelerated, extreme testing, not testing the highest possible pressure was acceptable.

3.5 Test Procedure

All samples were cleaned with acetone and weighed before testing. Once the cleaning process began, the samples were only handled with rubber gloves. The lower samples were numbered and used in order. The upper samples were chosen at random for each test. Before loading the samples into the UMT, the upper carriage was centered, and the force and torque sensors were manually and then electronically zeroed. Then, the upper samples were loaded into the UMT, followed by the lower sample. The test began after that. For the "with sand" tests, a five-minute pause was included after the load was applied in order to allow time to add the sand.

When the test ended, the samples were removed from the UMT. The samples were photographed before removal from the fixtures. Any sand or loose wear particles were discarded. The samples were cleaned with acetone before being weighed again. After the "with sand" tests, the fixtures, washers, spacers, and screws also had to be cleaned to remove any remaining sand on the parts and in the bolt holes. The initial and final weights were then recorded in a spreadsheet for further use. The data file generated by the UMT during the test was also downloaded.

Before and after photographs of a "no sand" test can be found in Figure 3.17. Photographs before and after removing the sand from a "with sand" test are in Figure 3.18. Both tests resulted in dark wear particles. The particles were visible as black particles in the "no sand" tests. In the "with sand" tests, the wear particles mixed into the sand to create a gray sandy mixture.

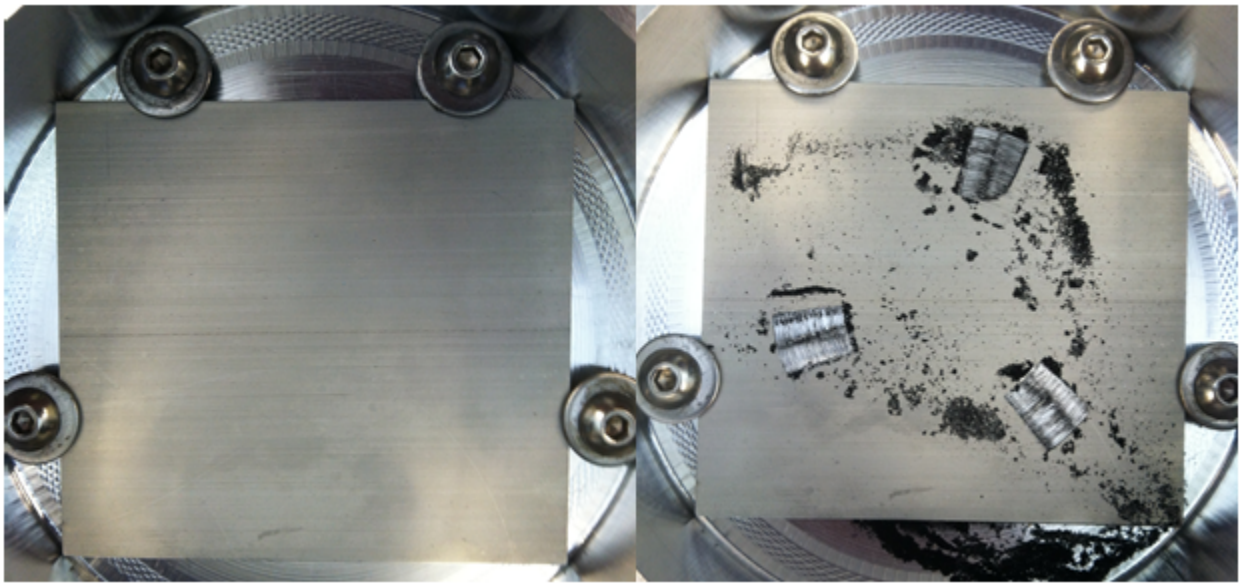

Figure 3.17: Before and after a "no sand" test

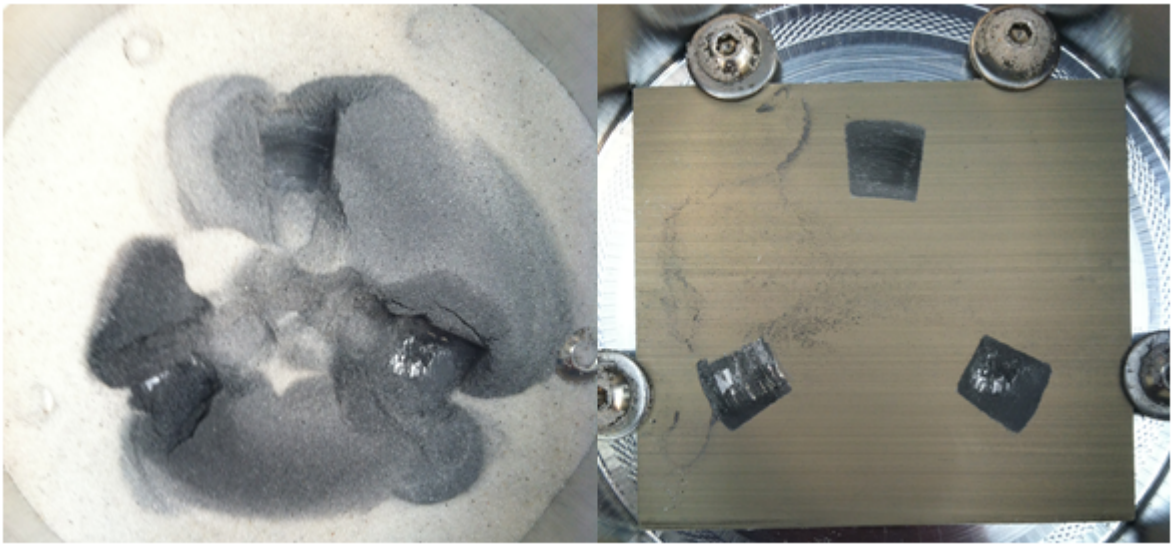

Figure 3.18: Before and after removing sand

3.6 Additional Tests

Three additional tests were run with the same samples and test configuration. Two of them were run with a change in the sand. The other test was performed to investigate where the black wear particles were coming from.

The first test was done with the foreign sand at a load of 150 N. The test was run as before, with the load applied before the sand was added.

The second series of tests used the Clearwater sand as before, but the sand was added before the surfaces came into contact and before the load was applied. The spaces between the lower sample and fixture were filled, and the surface of the sample was just barely covered uniformly. Five-thirds of a tablespoon of sand was used. Three loads were tested: 50 N, 150 N, and 250 N.

The third test was done to investigate what caused the black wear particles to form, specifically whether they were aluminum carbide formed by a reaction between the aluminum and the carbon dioxide in the atmosphere. The test was run at 100 N with unanodized samples. The samples adhered enough that they did not slide relative to each other for most of the test. There was less than 0.5 mg of mass lost on all of the samples.

Chapter 4

Results

4.1 Main Tests

Two methods of measuring wear were used for the main set of tests. The change in mass of both the upper and the lower samples was used to calculate the amount of wear and the wear rate. This method of measuring wear is known to work and is as accurate as the scale used to weigh the samples. The second method was to use the change in height of the upper carriage of the UMT to calculate the wear rate. This method has not been tested before, so the results should be compared to the weighing method to determine the validity of this method.

4.1.1 Change in Mass

Many of the articles discussed in the literature review used the weighing method to determine the wear rate of a set of materials [4, 7, 8, 9, 10, 11, 14, 18, 20, 21, 23, 28, 36, 37, 40]. The wear volume can be calculated from the known material density and the measured change in sample mass. Thus, the wear rate can be calculated as:

$$WR = \frac{\Delta V}{s} = \frac{\Delta m}{\rho s} \tag{4.1}$$

The sliding distance (s) is 27 m and the density (ρ) is 2.81 g/cm^3. The change in mass (Δm) for each lower sample or set of three upper samples is substituted from Tables 4.2 and 4.1, respectively.

	No Sand			Sand		
Load	Round 1	Round 2	Round 3	Round 1	Round 2	Round 3
50 N	-0.1	-0.1	-0.1	-14.1	-27.6	-24.4
100 N	-1.8	-2.7	-2.2	-24.2	-21.2	-22.2
150 N	-5.8	-4.4	-2.1	-44.1	-48.3	-55.8
200 N	-2.9	-2.5	-2.4	-16.2	-66.5	-54.4
250 N	-5.0	-0.3	-3.3	-25.6	-26.3	-64.2

Table 4.1: Test matrix with total mass lost from upper samples in mg

	No Sand			Sand		
Load	Round 1	Round 2	Round 3	Round 1	Round 2	Round 3
50 N	0.8	-2.4	-0.3	-9.3	-31.9	-27.0
100 N	-2.9	-2.5	-5.8	-24.9	-22.4	-28.9
150 N	-4.3	-9.0	-8.9	-50.6	-50.1	-56.9
200 N	-5.1	-5.6	-9.4	-22.7	-81.3	-53.3
250 N	-4.0	-0.7	-9.8	-30.6	-29.0	-61.4

Table 4.2: Test matrix with mass lost from lower samples in mg

4.1.2 Change in Height

It should be possible to calculate the wear rates from the change in volume of the upper samples. Since the contact area is assumed to be constant throughout the tests, the wear rate can be calculated from the change in sample height:

$$WR = \frac{\Delta V}{s} = \frac{\Delta h \; A}{s} \tag{4.2}$$

Accurately measuring the original and final heights of the samples with calipers would be ideal, but the calipers could damage the surfaces of the samples and affect the wear. As the sample height changes over the course of the test, the upper carriage of the UMT has to move to maintain the same contact force. This should mean that as the samples lose mass, the upper carriage should move down to compensate for the missing height. However, as can be seen in Figure 4.1 and in Appendix B, not only does the change in height appear to be random, sometimes it is positive, not negative. For the "with sand" tests, this is probably

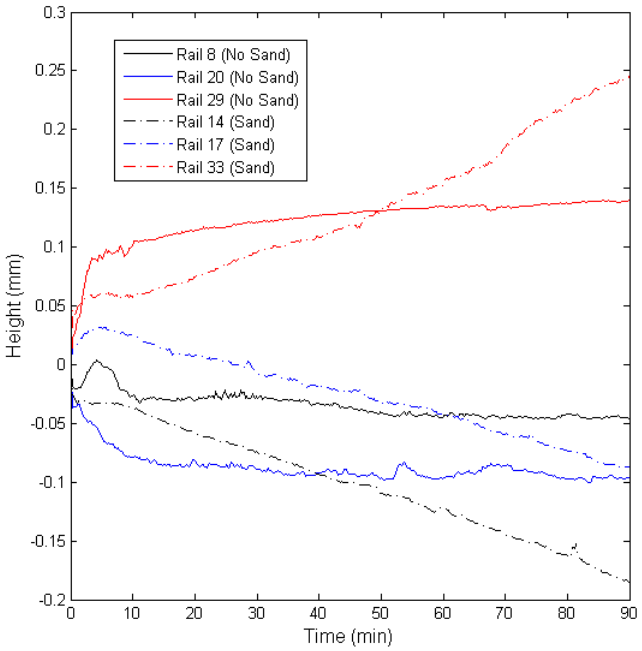

Figure 4.1: Change in height: 150 N

due to sand entering the contact and separating the surfaces. For the "no sand" tests, this may be due to the wear particles remaining in the contact.

4.1.3 Wear Rates

The wear rates from the changes in height and mass were calculated using Equations 4.1 and 4.2. The upper and lower sample mass wear rates in Figures 4.2 and 4.3 have a similar trend both with and without sand. The height-based wear rates in Figure 4.4 appear to follow the same trend when there is no sand, but the wear rates numerically come out to be negative. Additionally, there is little difference between the wear rates found for the "with sand" and "no sand" tests. Their ranges overlap and the averages are similar at nearly every load.

The average wear rates calculated from both mass changes and the height change are plotted together in Figure 4.5. The height-based wear rates are always much lower than the

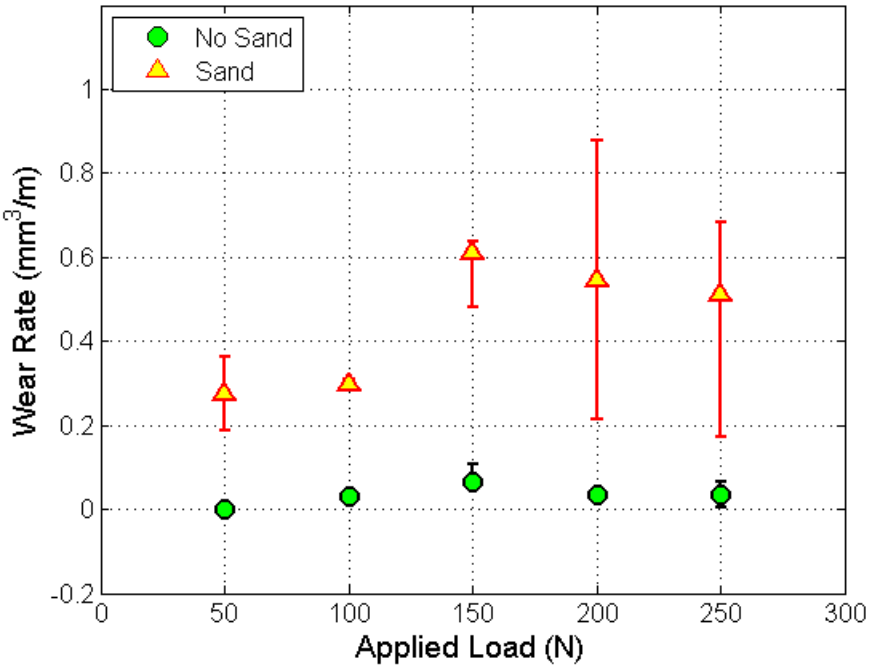

Figure 4.2: Wear rates from total change in upper sample mass

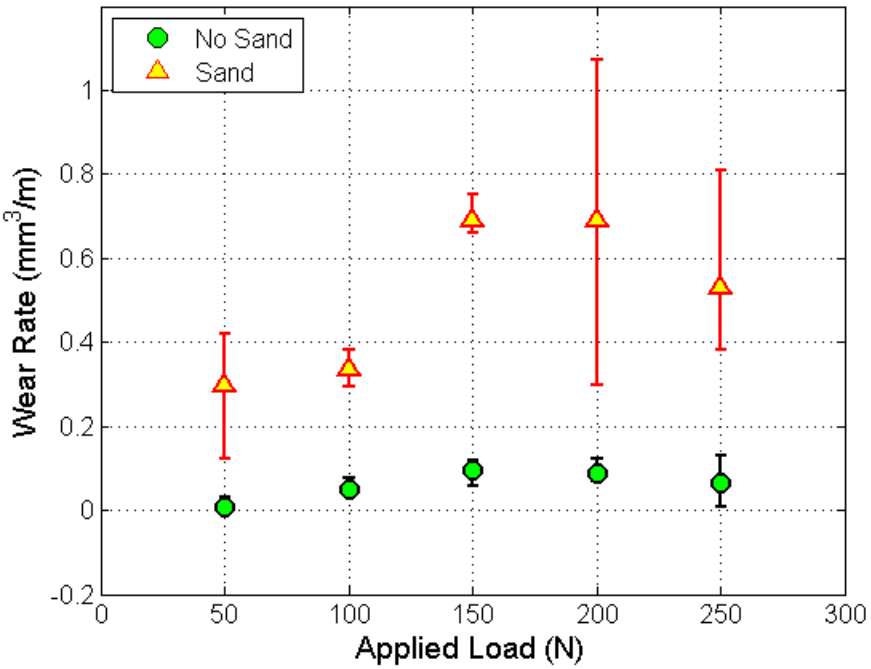

Figure 4.3: Wear rates from change in lower sample mass

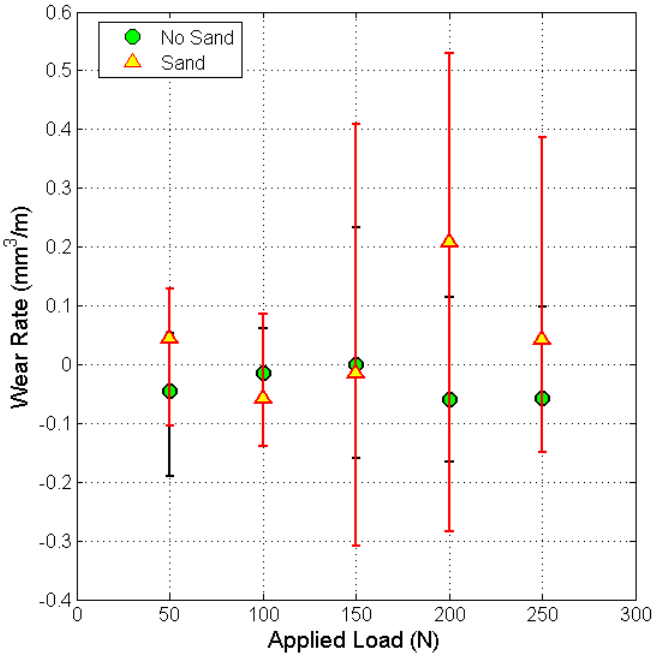

Figure 4.4: Wear rates from change in height

mass-based wear rates, especially in the case of the "no sand" wear rates, which are negative. The height-based sand wear rates are more similar to the "no sand" mass-based wear rates. Another interesting trend is apparent in this figure. The wear rates for the lower samples are always higher than the wear rates for the upper samples. The Type III anodization on the lower samples is about twice as thick as the Type II anodization on the upper samples, so this result is in agreement with Reference [23], which found that the wear rate actually increased with increasing anodic coating thickness.

4.2 Foreign Sand

A test was run with the foreign sand the same way as the original sand test: after the test began, there was a five-minute pause to add the foreign sand. The same amount of sand was used as the original tests. This sand was not sieved to remove other materials in order to avoid contaminating it with any beach sand that may have adhered to the sieve. The

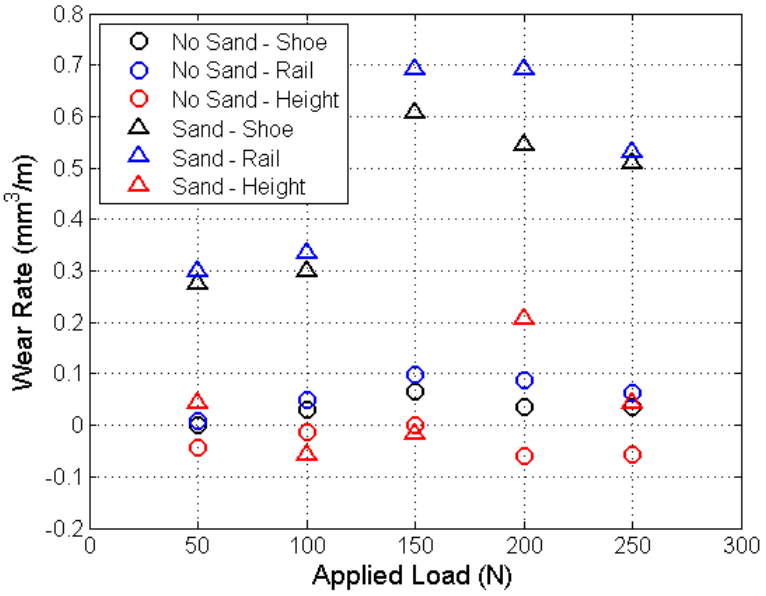

Figure 4.5: Average wear rates for all methods

sand tended to clump together, but much of it was loose. Figure 4.6 was taken at the end of the test. The sand grains adhered to each other so that very little sand entered the contact areas. The top left groove appeared to have almost no sand in it at any point during the test. The change in mass was also very low. There was slightly more wear than when no sand was present, but it was nowhere near as much as when the beach sand was added. This is most likely due to the sand sticking together and not entering the contact. Since the sand was collected by scraping it off parts, these grains are more likely to have an electrostatic charge, and there may have been other materials mixed into the sand like paint.

4.3 Sand before Loading

Adding the sand after the load caused more than ten times more wear in some cases, but submerging the samples in sand is not an accurate parallel with sand entering a mechanical system. A test with less sand might be more realistic. Additionally, having sand between the samples before applying the load would be similar to a situation where sand is on components

Figure 4.6: End of foreign sand test

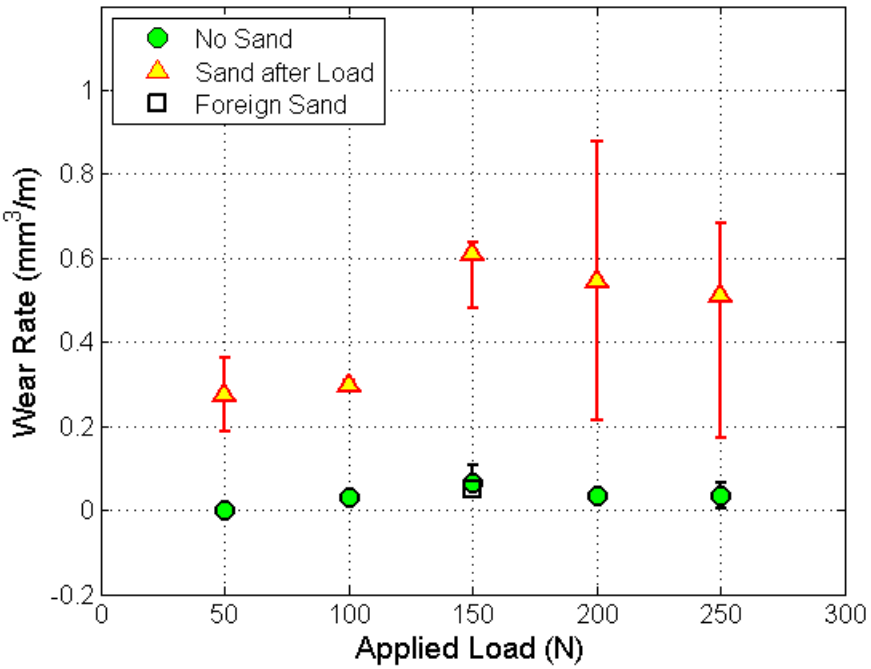

Figure 4.7: Wear rate from mass loss of upper samples for foreign sand

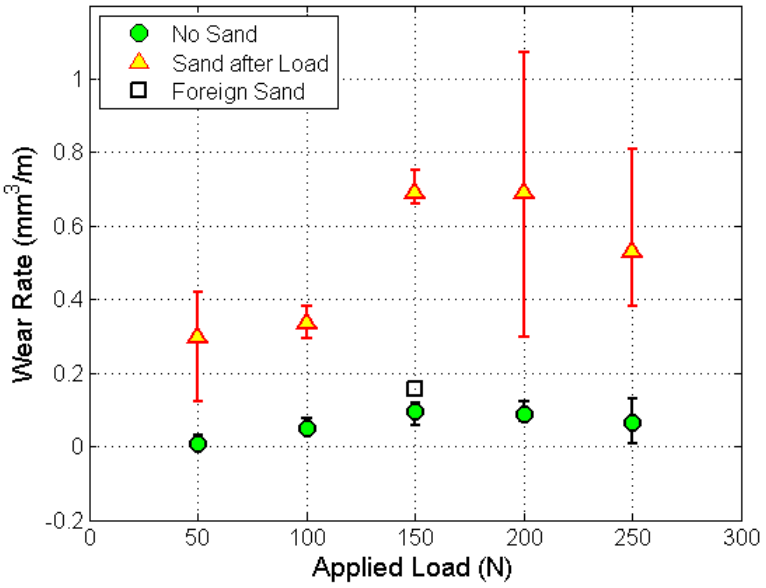

Figure 4.8: Wear rate from mass loss of lower samples for foreign sand

before they come into contact. A thin layer of sand was added over the lower sample before the load was applied for three loads (50 N, 150 N, 250 N) to test this.

4.3.1 Change in Mass

The goal of this test was to determine if adding the sand after the load was the best way to test the wear resistance of the anodization. The 50 N and 150 N tests were completed. The 250 N tests ended after 60 minutes due to the torque reaching the warning load of the torque sensor. The cause of this was investigated with profilometry and will be discussed later. The wear rates from the change in mass for these three cases are plotted with the wear rates from the change in mass from the main tests in Figures 4.10 and 4.9. Except for the rail sample at 50 N, this method does no cause much more wear than when there is no sand. Additionally, the wear grooves on these samples visually resemble the samples with no sand more than the samples submerged in sand.

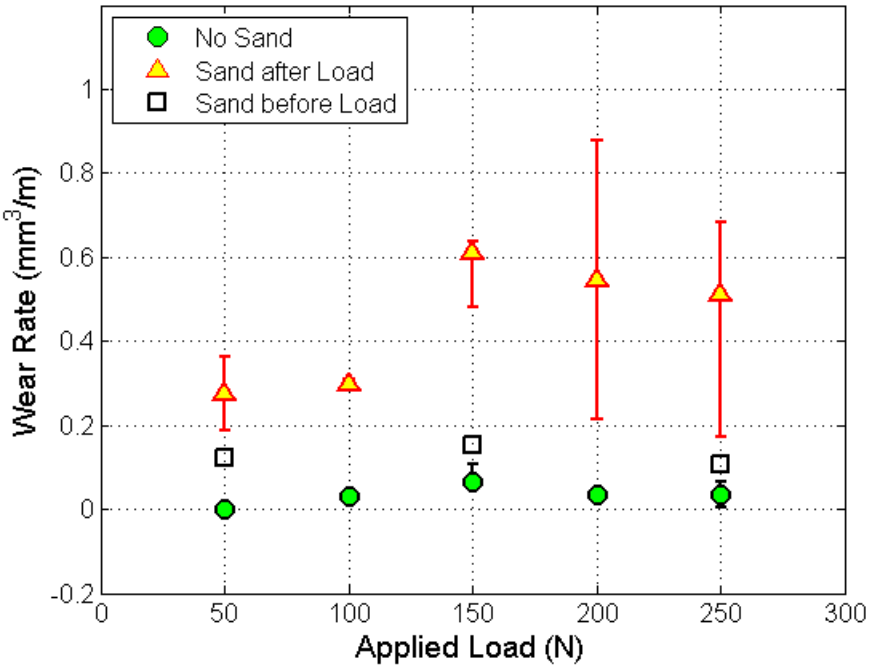

Figure 4.9: Wear rates from sand before loading - upper samples

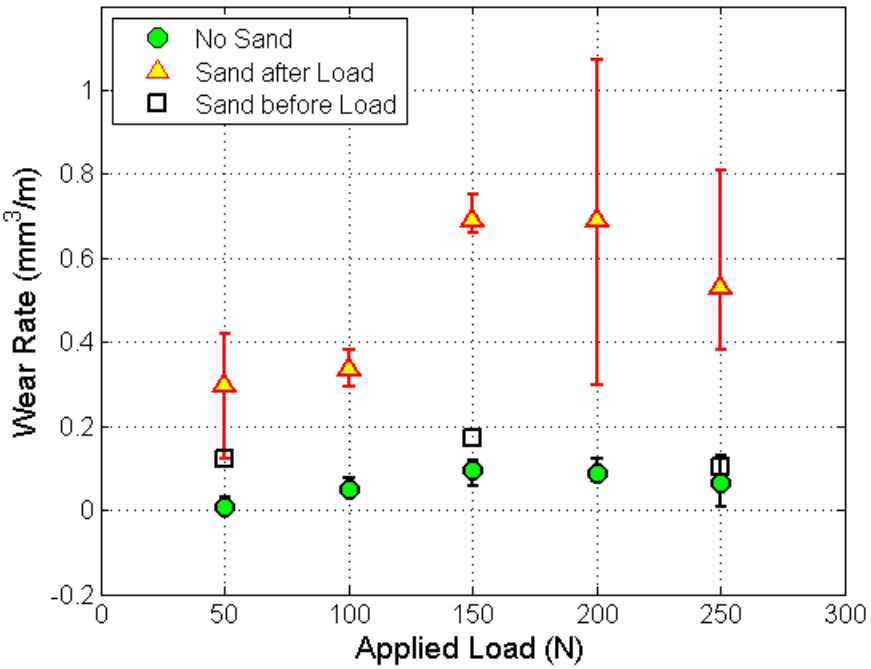

Figure 4.10: Wear rates from sand before loading - lower samples

4.3.2 Profilometry of Wear Grooves

A Veeco DEKTAK 150 stylus profilometer was used to study the wear grooves of three lower samples tested under different sand conditions at the same 250 N load. Since the third "sand before loading" test failed to run to completion, it was possible that an edge had formed in one of the grooves and caused the torque to rapidly increase.

Scan length (radial)	10 mm
Scan length (circumferential)	14 mm
Tip radius	25 μm
Vertical resolution	80 Å
Contact Force	10.00 mg

Table 4.3: Veeco DEKTAK 150 profilometer specifications

Figure 4.11: Veeco DEKTAK 150 stylus profilometer

Each of the wear grooves on each sample was scanned six times: three parallel to the sliding direction (circumferential) and three perpendicular to the sliding direction (radial). A diagram of where these scans were taken can be found in Figure 4.12.

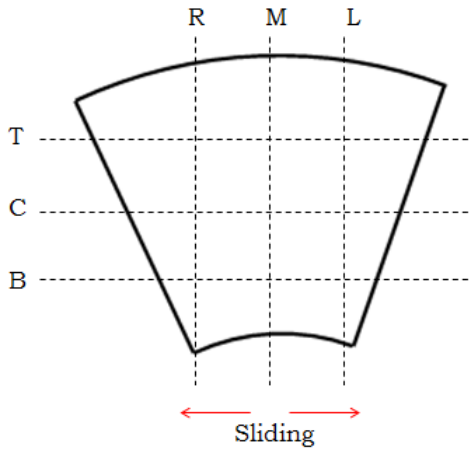

Figure 4.12: Diagram of profile locations

The depths of each groove and the roughnesses of surfaces within the grooves were compared. The RMS roughness (R_q) of the wear grooves was calculated as:

$$R_q = \left(\frac{1}{n} \sum_{i=1}^{n} z_i^2 \right)^{\frac{1}{2}} \tag{4.3}$$

Figures 4.13 and 4.14 show the R_q for the radial and circumferential profiles, respectively. The bars represent the roughness of each profile; the blue circles represent the averages for each of the three grooves on the samples; and the yellow squares represent the average of all profiles in that direction for the sample. The roughnesses of the "no sand" and "sand before loading" samples were very similar, especially in the parallel direction. The "sand after loading" sample was three times as rough as the "no sand" sample in the radial direction and six times as rough in the circumferential direction.

The samples tested without sand and with the sand added before the load have similar depths. The samples tested with the sand added after the load had significantly deeper grooves. This shows that the torque cutoff was most likely from a problem with the torque sensor itself, not a product of the samples getting stuck together.

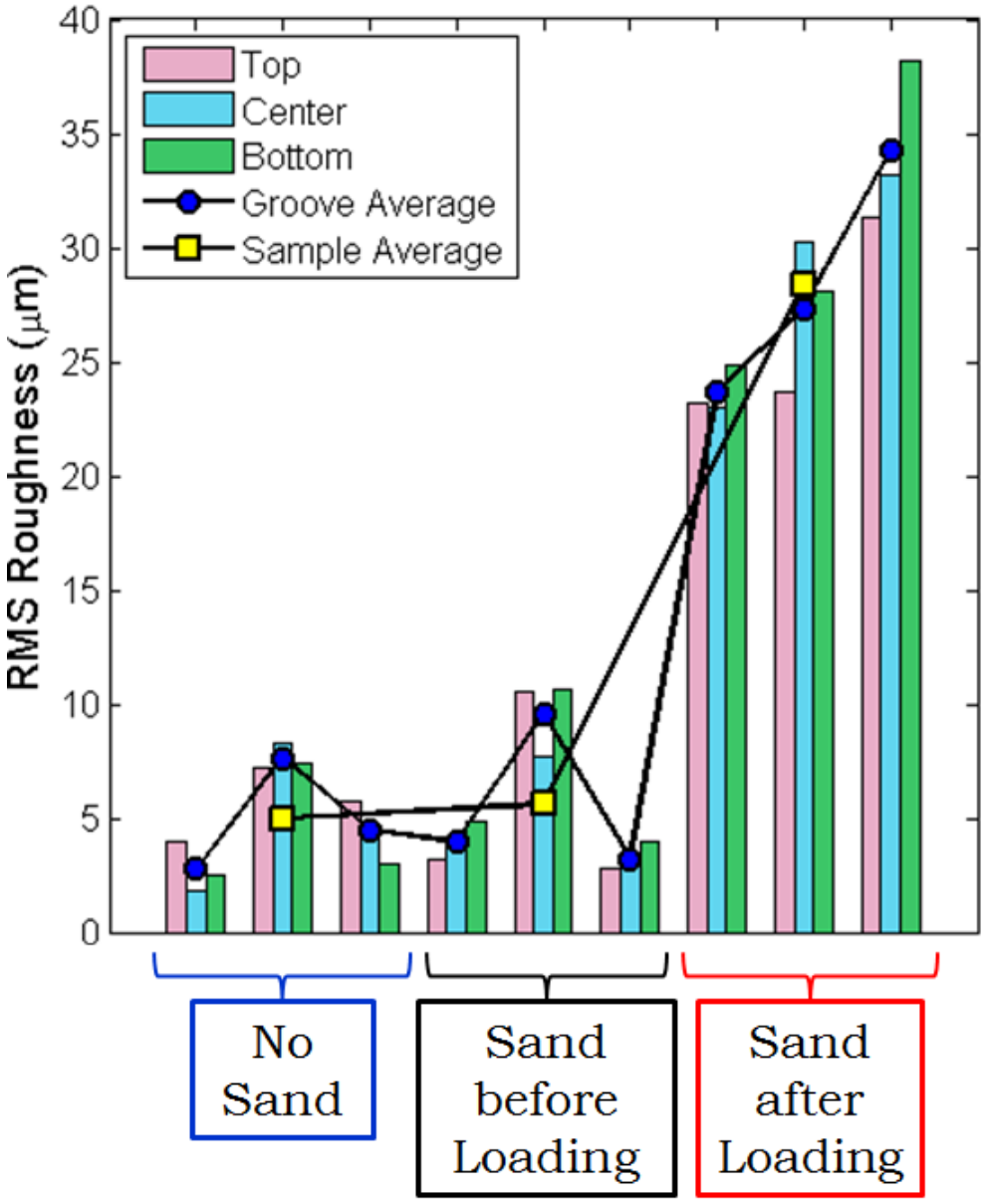

Figure 4.13: Radial RMS roughness

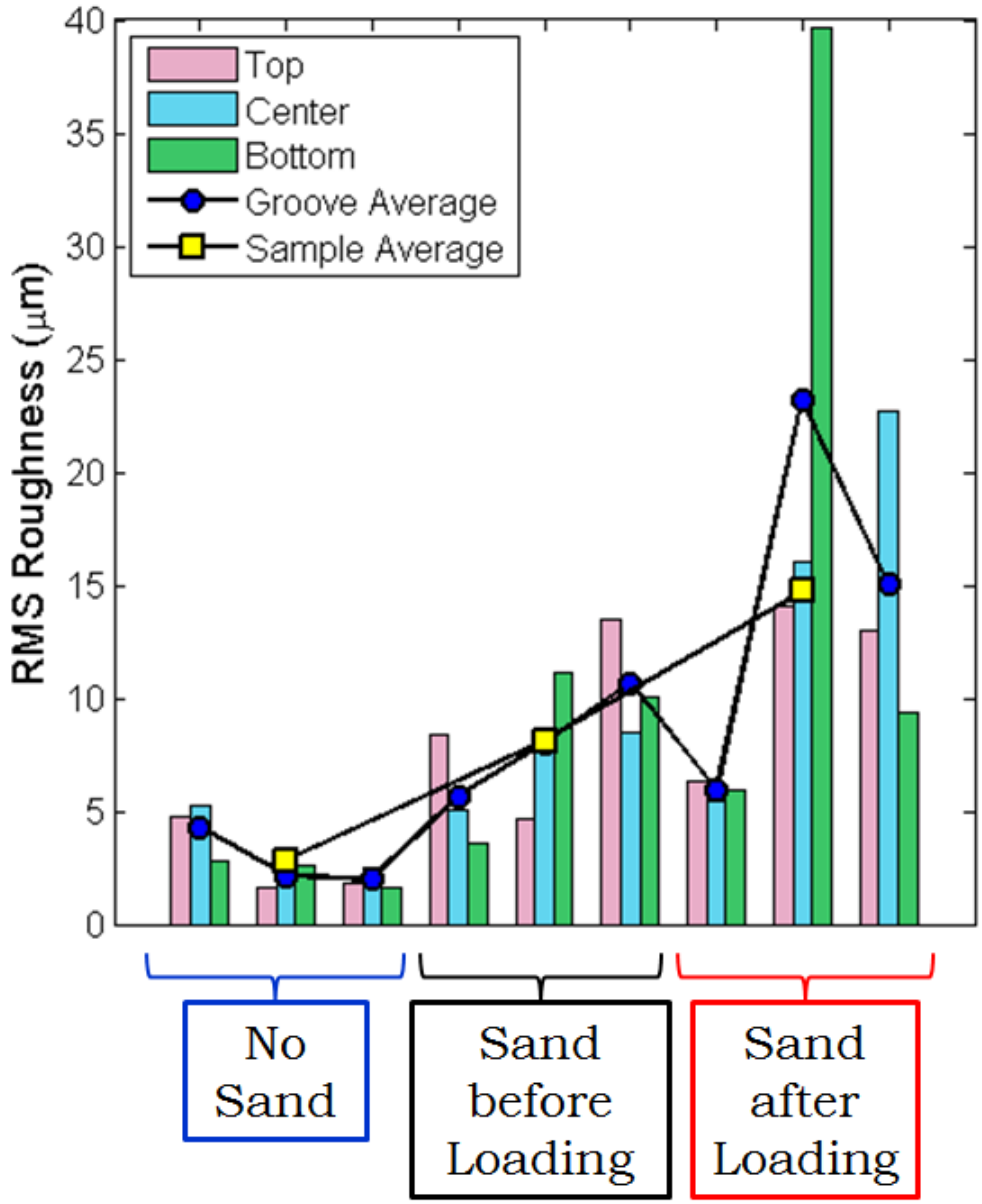

Figure 4.14: Circumferential RMS roughness

Chapter 5

Conclusion

In this thesis, the effect of sand on the wear of anodized aluminum was examined. The angularity and size of the sand were important factors, and care was taken to control the size of the grains. The sand had to be free of other debris and particles. The test with the foreign sand did not have the expected results because the sand tended to adhere to other materials that were in the sand sample.

The method of adding the sand to the experiment is also important. When a thin layer of sand was used to cover the lower sample prior to applying the load, most of the sand was swept out of the contact areas. The resulting wear was not much more severe than when there was no sand, which was evident both in the wear rate and in the similar roughness in the wear grooves. Submerging the wear system in the sand allowed the sand to feed into the contact areas throughout the duration of the tests. This increased the wear rates of the anodized samples by an order of magnitude compared to when there was no sand. The sand also increased the roughness of the wear grooves by 3 to 5 times. These increases are most likely due to the dominant wear mechanism of the system changing from an adhesive mechanism without sand to a three-body abrasive mechanism with sand.

The change in the mass of the samples is the best method for measuring wear rates. The change in sample height as measured by the UMT was inconsistent. The height-based wear rates were similar without sand and with sand, which should not be the case. For all cases, a non-linear relationship between wear rate and applied load was observed. Therefore, these materials do not follow Archard's equation (Equation 2.2).

The source of the wear particles is still unknown. Since the same particles formed with and without anodization, the particles are not a product of the anodic coating. The particles

are either a product of the aluminum alloy itself or a reaction of the aluminum with carbon dioxide in the air.

5.1 Future Work

The next step is to run the same series of tests with a coating on the upper samples. Several possibilities exist, such as Type III anodization, diamond-like carbon (DLC), tungsten carbide (WC), and microarc oxidation (MAO). Type III anodization is formed like Type II, but it is more than twice as thick [26]. It would last longer, but the wear rate would increase. A DLC or WC coating would decrease the wear. However, WC coatings tend to fail due to delamination and have adhesion problems [5]. DLC coatings have varying properties which can depend on how the coating is deposited, the hydrogen in the coating, and environmental factors such as humidity and temperature, among other variables. The friction of the coating also depends on the roughness of the surface it is applied to [15]. MAO is the most viable option. The process is similar to anodization, but the oxide layer that forms is nonporous and similar in character to a ceramic. It has been shown to decrease the wear of uncoated aluminum by a factor of 12, compared to a factor of 2 by hard coat anodization [20].

In order to continue investigating the black wear particles, a test will be run in a carbon dioxide-free environment. A gas mixture of 21% oxygen and 79% nitrogen will be fed into a glove bag containing the UMT and a set of samples. If no wear particles form, then the reaction is caused be carbon dioxide in the air.

Bibliography

[1] Aerts, T., Th. Dimogerontakis, I. De Graeve, J. Fransaer, and H. Terryn, *Influence of the anodizing temperature on the porosity and the mechanical properties of the porous anodic oxide film*, Surface Coatings and Technology, 2007. 201(16-17): pp. 7310-7317.

[2] Archard, J.F., *Contact and Rubbing of Flat Surfaces*, Journal of Applied Physics, 1953. 24(8).

[3] Archard, J.F., *Elastic deformation and the laws of friction*, Proceedings of the Royal Society of London. Series A, Mathematical and Physical Sciences, 1957. 243(1233): pp. 190-205.

[4] Archard, J.F. and W. Hirst, *The wear of metals under unlubricated conditions*, Proceedings of the Royal Society of London. Series A, Mathematical and Physical Sciences, 1956. 236(1206): pp. 397-410.

[5] Bahadur, S. and C.N. Yang, *Friction and wear behavior of tungsten and titanium carbide coatings*, Wear, 1996. 196(1-2): pp. 156-163.

[6] Barnes, Graham, Soil Mechanics: Principles and Practice, 3rd edition, Palgrave Macmillan, 2010. pp. 1-26

[7] Bensalah, W., K. Elleuch, M. Feki, M. Wery, and H.F. Ayedi, *Mechanical and Abrasive Wear Properties of Anodic Oxide Layers Formed on Aluminium*, Journal of Materials Science and Technology, 2009. 25(4): pp. 508-512.

[8] Bingley, M.S. and S. Schnee, *A study of the mechanisms of abrasive wear for ductile metals under wet and dry three-body conditions*, Wear, 2005. 258(1-4): pp. 50-61.

[9] Campbell, A., W. Mortimer, and P. Thornton, *The Abrasion Characteristics of Certain Protective Coatings on Aluminum and Magnesium Alloys*, US Army Armament Research and Development Command, 1977.

[10] Cheng, B.R. and L. Hao, *Comparative Study of the Effects of Sealing Processes on the Wear Resistance and the Sealing Quality of Hard Anodic Coatings*, Metal Finishing, 2000. 98(5): pp. 48-55.

[11] Chou, S.M. and H. Leidheiser, Jr., *Wear of Anodized Aluminum under Three-Body Conditions*, Industrial & Engineering Chemistry Product Research and Development, 1986. 25(3): pp. 473-478.

[12] Department of Defense Test Method Standard MIL-STD-810G, *Environmental Engineering Considerations and Laboratory Tests*, 2008.

[13] Du, L., B. Xu, S. Dong, H. Yang, and W. Tu, *Study of tribological characteristics and wear mechanism of nano-particle strengthened nickel-based composite coatings under abrasive contaminant lubrication*, Wear, 2004. 257(9-10): pp. 1058-1063.

[14] Emeric, D.A., S. Levine, and K.L. Washburn, *The Effect of Surface Coatings on the Fatigue Strength of Aluminum Alloys*, US Army Mobility Equipment Research and Development Command, 1981.

[15] Erdemir, A. and C. Donnet, *Tribology of diamond-like carbon films: recent progress and future prospects*, Journal of Physics D: Applied Physics, 2006. 39(18): pp. R311-R327.

[16] Federal Test Method Standard Number 141C, *Paint, Varnish, Lacquer, and Related Materials; Methods for Sampling and Testing*, 1986.

[17] Ferguson, D.C., D.M. Wilt, A.F. Hepp, J.C. Kolecki, M.W. Siebert, P.P. Jenkins, D.A. Scheiman, N.S. Fatemi, and R.W. Hoffman, Jr., *The Mars Pathfinder Wheel Abrasion Experiment*, Materials and Design, 2001. 22(7): pp. 555-564.

[18] Fernández, J.E., M.d.R. Fernández, R.V. Diaz, and R.T. Navarro, *Abrasive wear analysis using factorial experiment design*, Wear, 2003. 255(1-6): pp. 28-43.

[19] Gao, J., C. Chen, G.T. Flowers, R.L. Jackson, and M.J. Bozack, *The Influence of Particulate Contaminants on Vibration-Induced Fretting Degradation in Electrical Connectors*, Proceedings of the 56th IEEE Holm Conference on Electrical Contacts, Charleston, SC, 2010.

[20] Krishna, L.R., A.S. Purnima, and G. Sundararajan, *A comparative study of tribological behavior of microarc oxidation and hard-anodized coatings*, Wear, 2006. 261(10): pp. 1095-1101.

[21] Kumar, S., A.P. Harsha, H.S. Goyal, A.A. Hussain, and S.B. Wesley, *Three-body abrasive wear behaviour of aluminium alloys*, Journal of Engineering Tribology, 2013. 227(4): pp. 328-338.

[22] Li, C. and F. Yan, *Effect of Blowing Air and Floating Sand-dust Particles on the Friction and Wear Behavior of PTFE, UHMWPE, and PI*, Tribology Letters, 2008. 32(3): pp. 189-198.

[23] Markowitz, L., *Hard Anodic Coatings on Aluminum Alloys: Evaluation and Control of Porosity*, Metal Finishing, 1992. 90(19): pp. 19-24.

[24] Mehta, D.S., S.H. Masood, W.Q. Song, *Investigation of wear properties of magnesium and aluminum alloys for automotive applications*, Journal of Materials Processing Technology, 2004. 156(1): pp. 1526-1531.

[25] Metals Handbook, 2nd edition, ASM International, 1998.

[26] Military Specification MIL-A-8625F, *Anodic Coatings, for Aluminum and Aluminum Alloys*, 1993.

[27] Noble, J.W., III and H. Leidheiser, Jr., *Wear of Anodized Aluminum-Polymer Lithographic Printing Plates*, Industrial & Engineering Chemistry Product Research and Development, 1981. 20(2): pp. 344-350.

[28] Nuruzzaman, D.M. and M.A. Chowdhury, *Friction Coefficient and Wear Rate of Copper and Aluminum Sliding against Mild Steel*, International Transaction Journal of Engineering, Management, & Applied Sciences & Technologies, 2012. 4(1): pp. 29-40.

[29] PGA TOUR, *Course Conditioning Guidelines*, pp. 4-5.

[30] Powers, M.C., *A New Roundness Scale for Sedimentary Particles*, Journal of Sedimentary Petrology, 1953. 23(2): pp. 117-119.

[31] Quercia, G., I. Grigorescu, H. Contreras, C. Di Rauso, and D. Gutiérrez-Campos, *Friction and wear behavior of several hard materials*, International Journal of Refractory Metals & Hard Materials, 2001. 19(4-6): pp. 359-369.

[32] Rabinowicz, Ernest Friction and Wear of Materials, 2nd edition, John Wiley & Sons, Inc., 1995.

[33] Riddar, F., S. Hogmark, and A.K. Rudolphi, *Comparison of anodised aluminium surfaces from four fabrication methods*, Journal of Materials Processing Technology, 2012. 212(11): pp. 2272-2281.

[34] Sadeler, R., S. Atasoy, A. Arici, and Y. Totik, *The Fretting Fatigue of Commercial Hard Anodized Aluminum Alloy*, Journal of Materials Engineering and Performance, 2009. 18(9): pp. 1280-1284.

[35] Sibert, M.W., *Wheel Abrasion Ground Tests: Initial Results*, Proceedings of the 32nd Intersociety Energy Conversion Engineering Conference, Honolulu, HI, 1997.

[36] Spuzic, S., M. Zec, K. Abhary, R. Ghomashchi, and I. Reid, *Fractional design of experiments applied to a wear simulation*, Wear, 1997. 212(1): pp. 131-139.

[37] Stachowiak, G.B. and G.W. Stachowiak, *The effects of particle characteristics on three-body abrasive wear*, Wear, 2001. 249(3-4): pp. 201-207.

[38] Tonghai, W., D. Dongfeng, and F. Liang, *Abrasive Wear Mechanisms of Sand Particles Intruding into ATM Roller-Scraper Tribosystem*, Chinese Journal of Mechanical Engineering, 2009. 22(3).

[39] Trezona, R.I. and I.M. Hutchings, *Three-body abrasive wear testing of soft materials*, Wear, 1999. 233(1): pp. 209-221.

[40] Westre, T., B.R. Cheng, L. Hao, and S. Westre, *Performance Results for Sealed Type III Anodic Oxides*, METALAST International, Inc., 2001.

[41] Williamson, J.B.P., J.A. Greenwood, and J. Harris, *The influence of dust particles on the contact of solids*, Proceedings of the Royal Society of London. Series A, Mathematical and Physical Sciences, 1956. 237(1211): pp. 560-573.

Appendices

Appendix A

MATLAB^{TM} Image Processing Code

```
clear all; close all; clc
name = 'CSand6.xls';
data1 = imread('6.JPG');
data = rgb2gray(data1);
fig1= figure;
imshow(data)
%% Trim
data1 = data1(:,:,1);
fig1_5 = figure;
imshow(data)
%% Changing the Contrast
g = graythresh (data);
Contrast_option = vision.ContrastAdjuster('InputRange','Custom',...
    'CustomInputRange', [220 , 245] );
I3 = step( Contrast_option , data );
%% Denoising
I4 = bwareaopen(I3, 1500);
fig2 = figure;
imshow(I4)
%% Finding the Boundary
I5 = bwboundaries(I4, 'noholes');
l=1;
for j=1:length(I5)
    for k=1:length(I5{j});
        x{j}(k) = I5{j}(k,1);
```

```
        y{j}(k) = I5{j}(k,2);
        data1 (x{j}(k), y{j}(k), 1) = 255;
        data1 (x{j}(k), y{j}(k), 2) = 255;
        data1 (x{j}(k), y{j}(k), 3) = 0;
        l = l + 1;
    end
end
fig3 = figure;
imshow(data1)
hold on
%% Center of the Area of each Grain
for j =1:length(I5)
    x_c(j) = sum(x{j}(:))/length(x{j});
    y_c(j) = sum(y{j}(:))/length(y{j});
end
plot(y_c,x_c,'db','MarkerFaceColor','g','MarkerSize',8)
%% Finding the Radius
for j =1:length(I5)
   r(j) = sum(((x{j}(:)-x_c(j)).^2 + (y{j}(:)-y_c(j)).^2).^.5)/length(x{j});
end
SF = 1e-3/(1143-569);
r = r*SF;
R_avg = sum(r(:))/length(r);
fprintf('Average Radius = %g',R_avg)
fprintf('(m)')
fprintf('\n')
fprintf('Average Diameter = %g',2*R_avg)
fprintf('(m)')
fprintf('\n')
xlswrite(name,transpose(r))
```

Appendix B

Change in Height Graphs

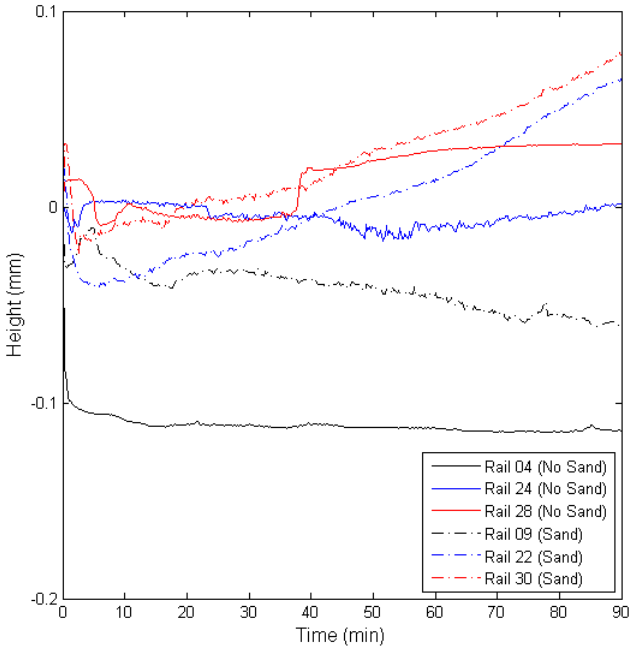

Figure B.1: Change in height: 50 N

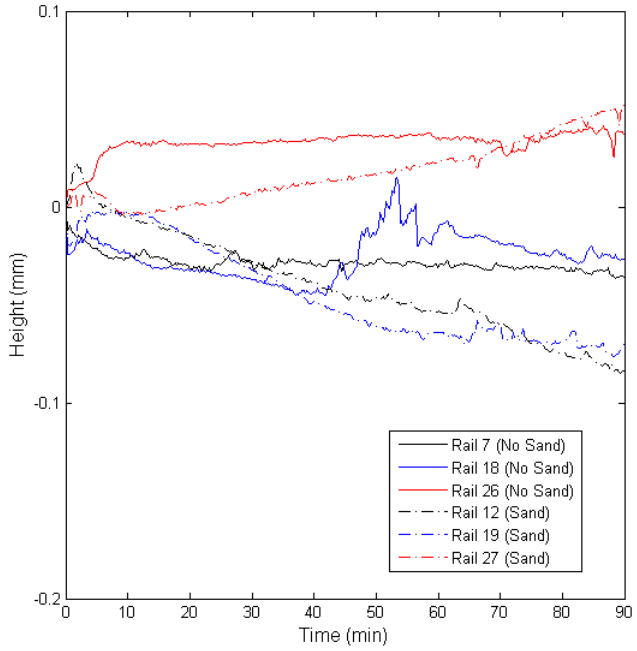

Figure B.2: Change in height: 100 N

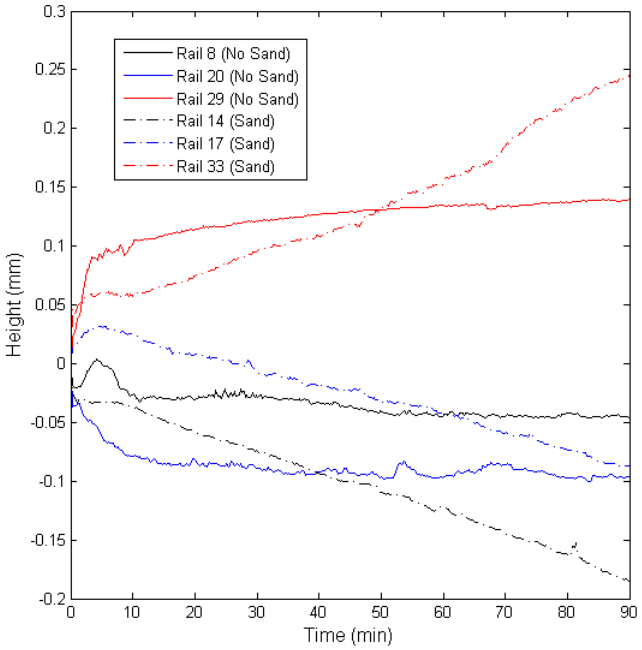

Figure B.3: Change in height: 150 N

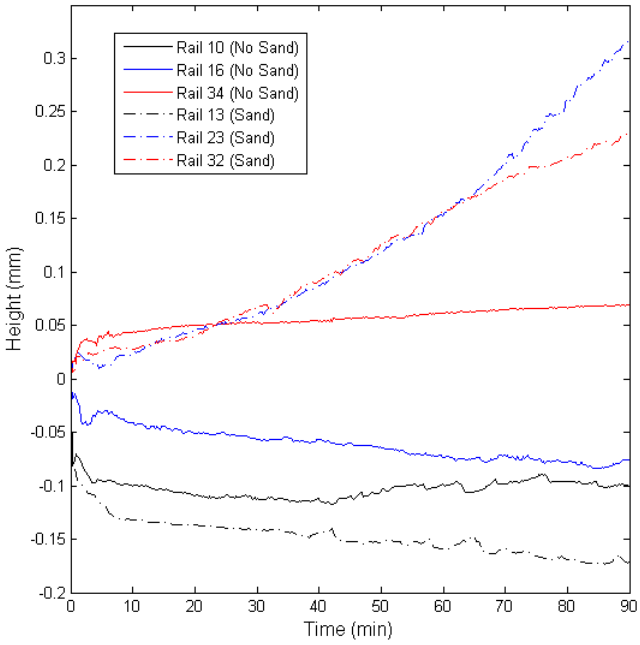

Figure B.4: Change in height: 200 N

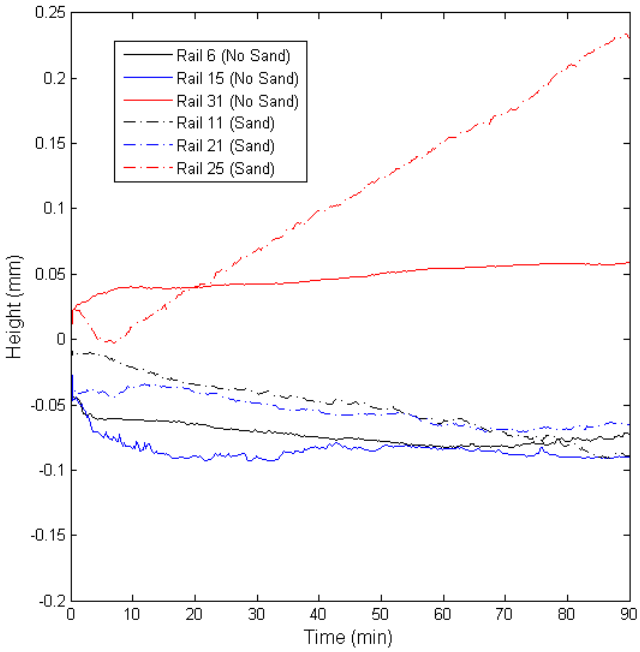

Figure B.5: Change in height: 250 N

Appendix C

Torque Plots

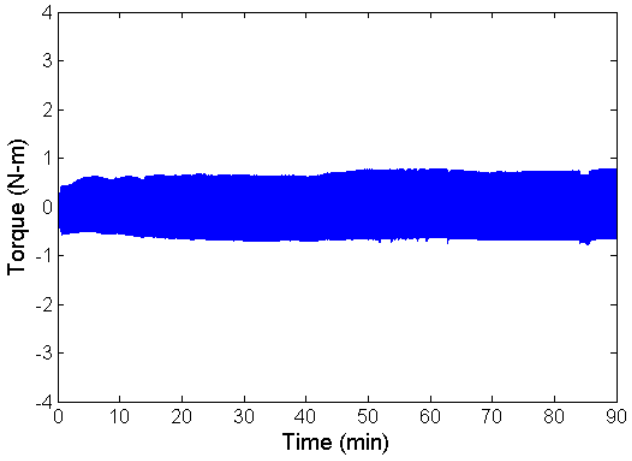

Figure C.1: Sample 4: 50 N, no sand

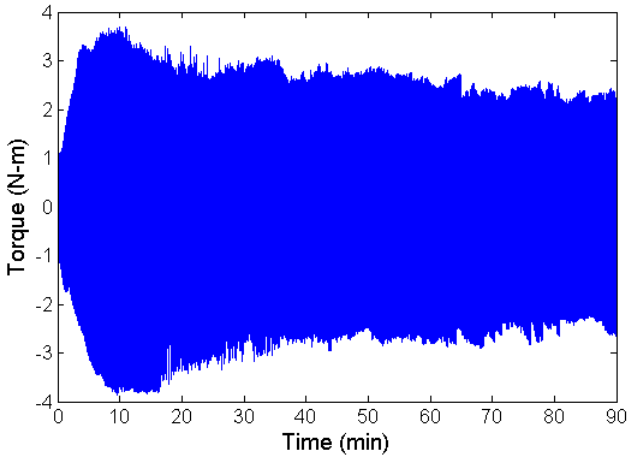

Figure C.2: Sample 6: 250 N, no sand

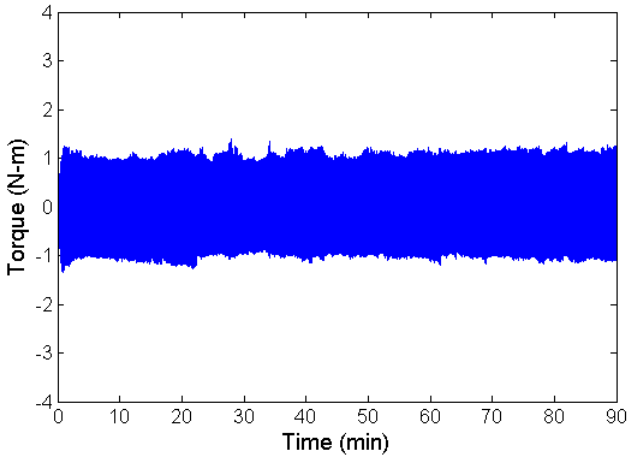

Figure C.3: Sample 7: 100 N, no sand

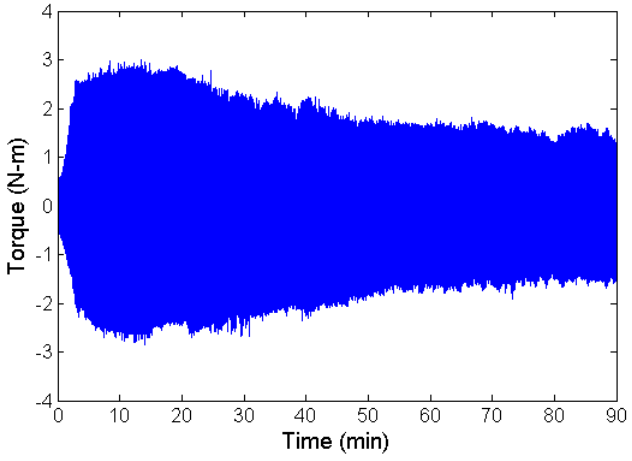

Figure C.4: Sample 8: 150 N, no sand

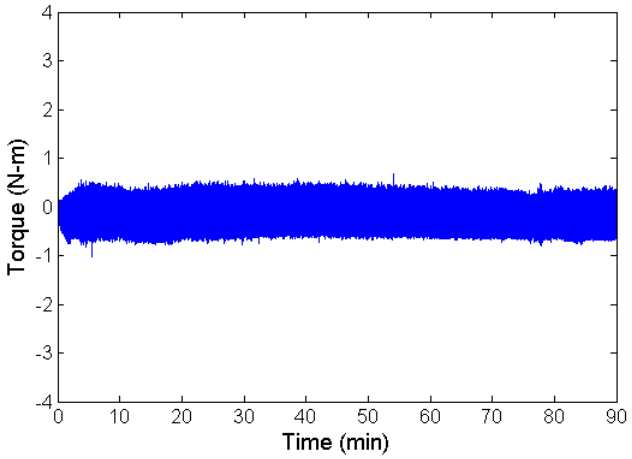

Figure C.5: Sample 9: 50 N, with sand

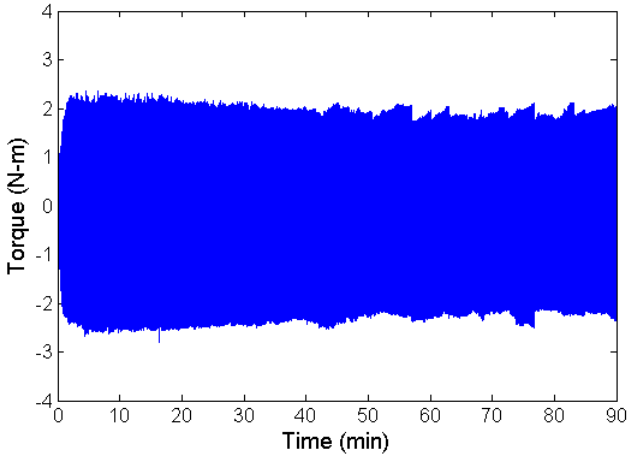

Figure C.6: Sample 10: 200 N, no sand

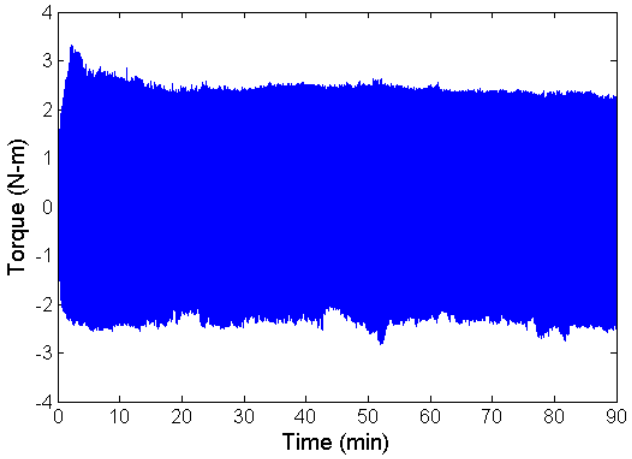

Figure C.7: Sample 11: 250 N, with sand

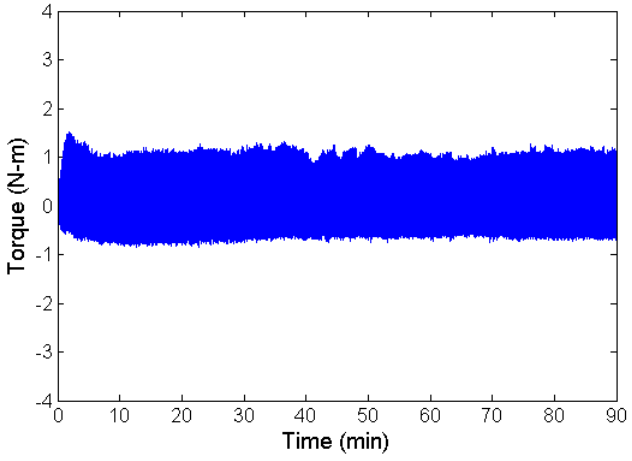

Figure C.8: Sample 12: 100 N, with sand

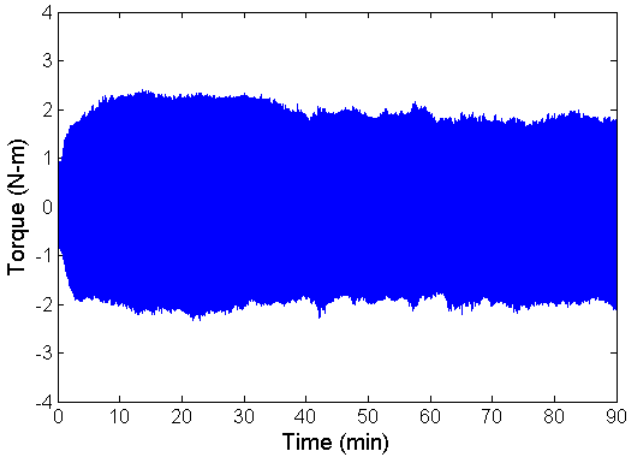

Figure C.9: Sample 13: 200 N, with sand

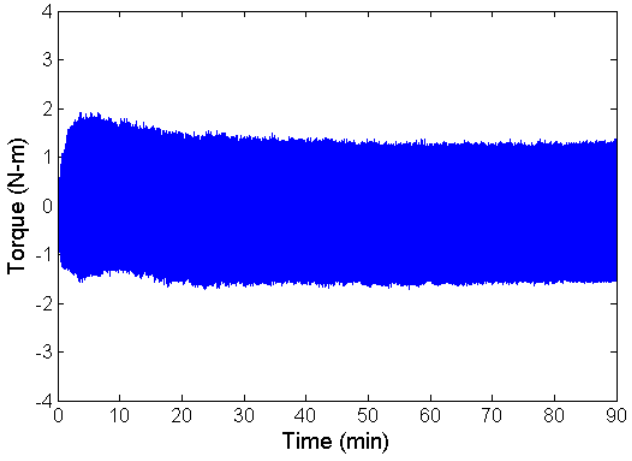

Figure C.10: Sample 14: 150 N, with sand

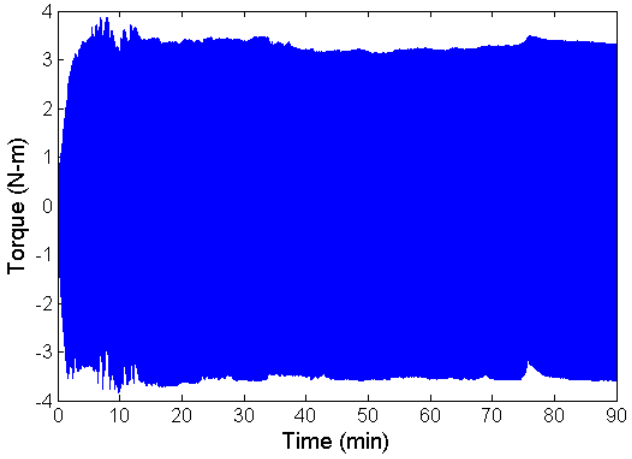

Figure C.11: Sample 15: 250 N, no sand

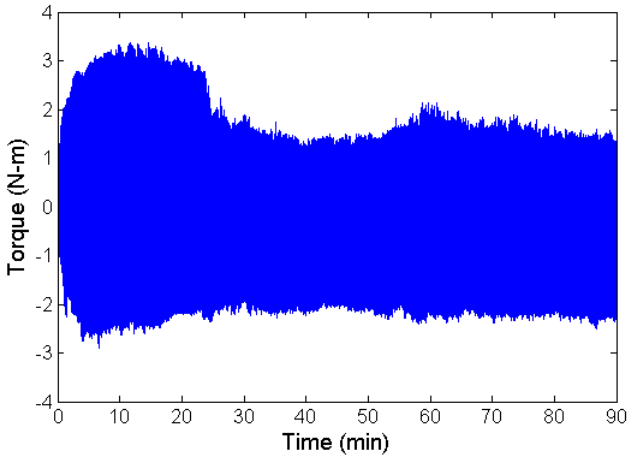

Figure C.12: Sample 16: 200 N, no sand

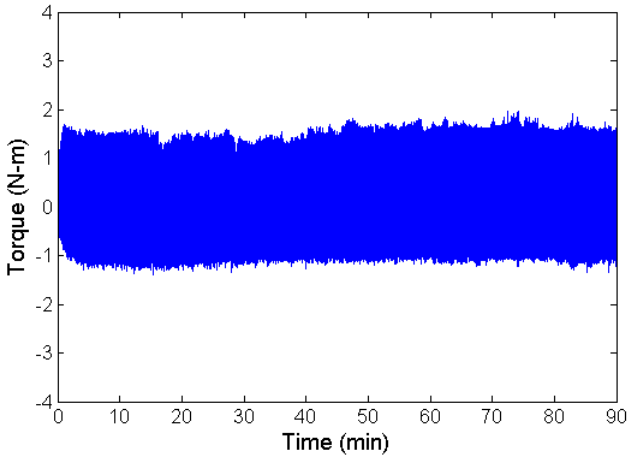

Figure C.13: Sample 17: 150 N, with sand

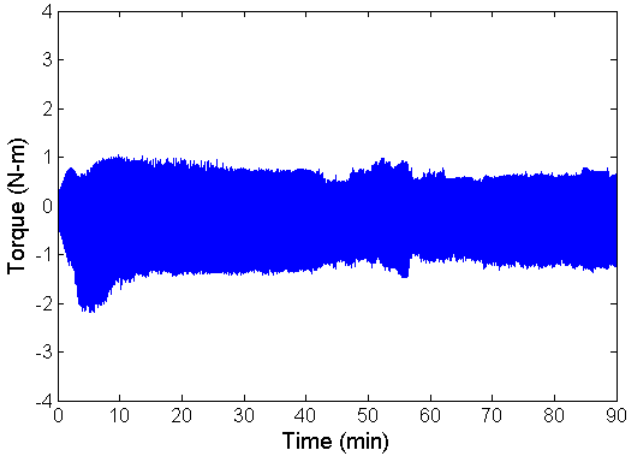

Figure C.14: Sample 18: 100 N, no sand

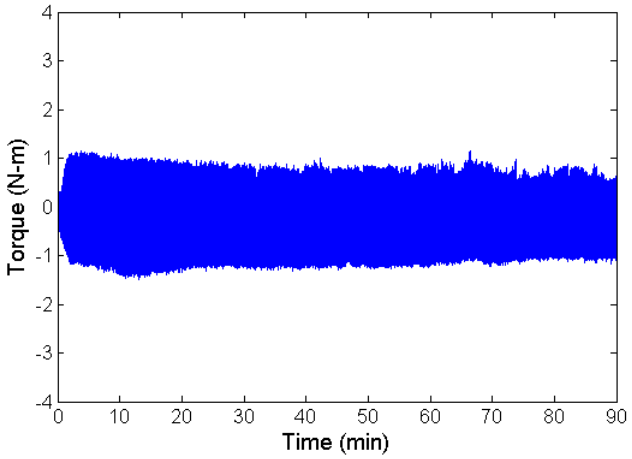

Figure C.15: Sample 19: 100 N, with sand

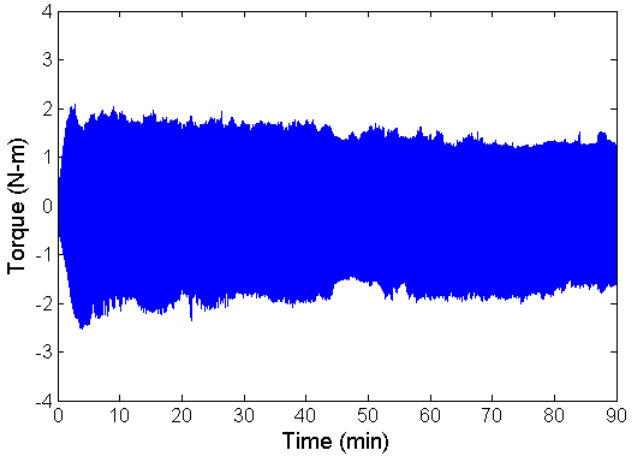

Figure C.16: Sample 20: 150 N, no sand

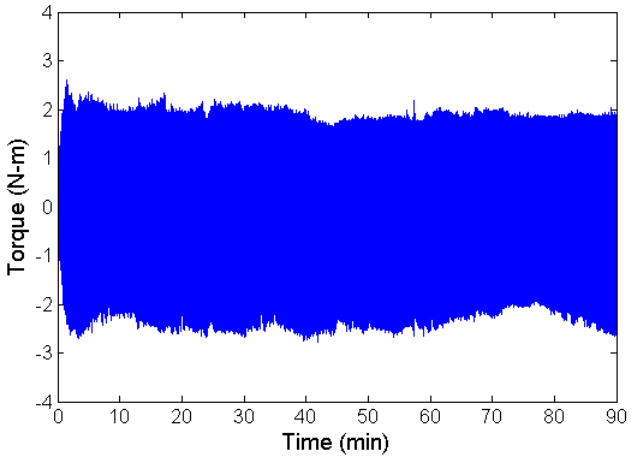

Figure C.17: Sample 21: 250 N, with sand

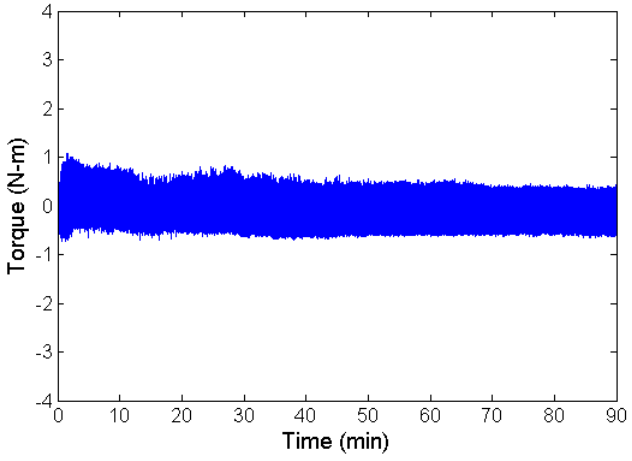

Figure C.18: Sample 22: 50 N, with sand

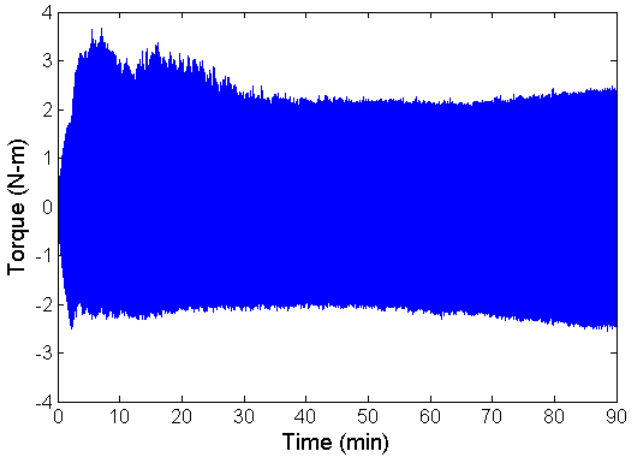

Figure C.19: Sample 23: 200 N, with sand

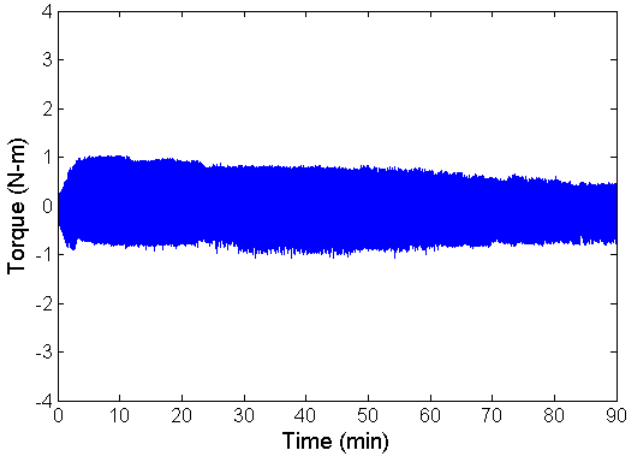

Figure C.20: Sample 24: 50 N, no sand

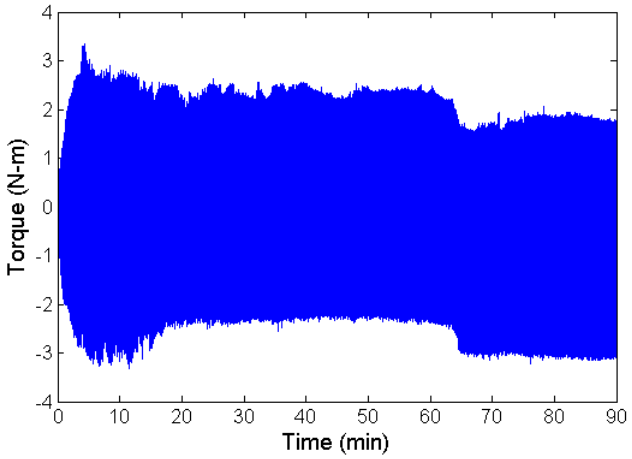

Figure C.21: Sample 25: 250 N, with sand

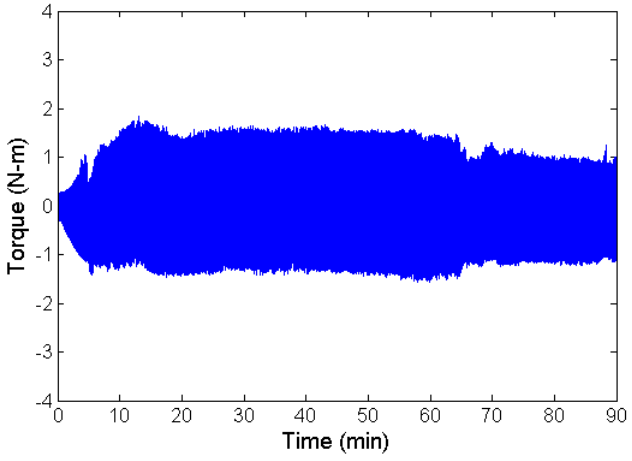

Figure C.22: Sample 26: 100 N, no sand

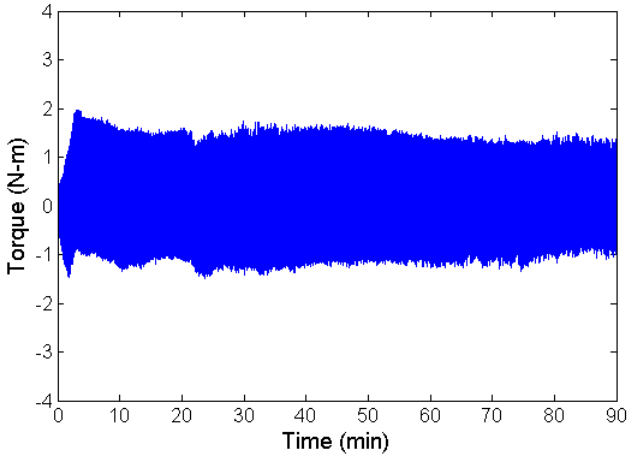

Figure C.23: Sample 27: 100 N, with sand

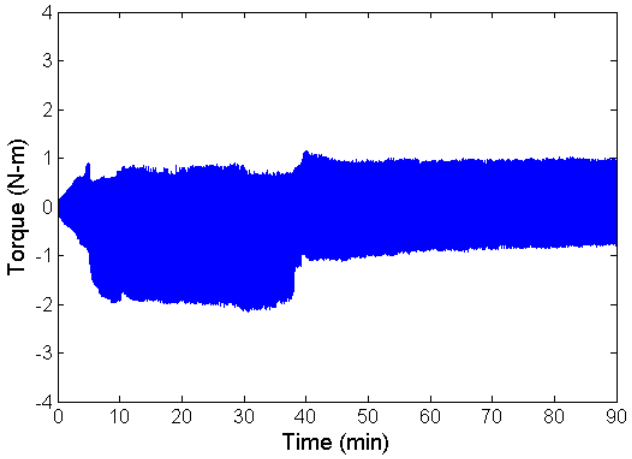

Figure C.24: Sample 28: 50 N, no sand

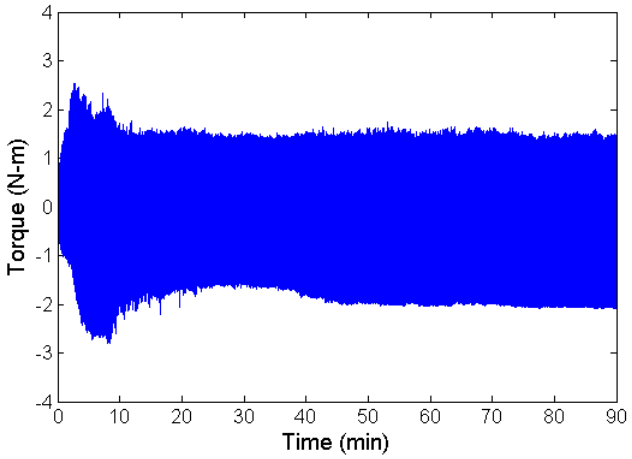

Figure C.25: Sample 29: 150 N, no sand

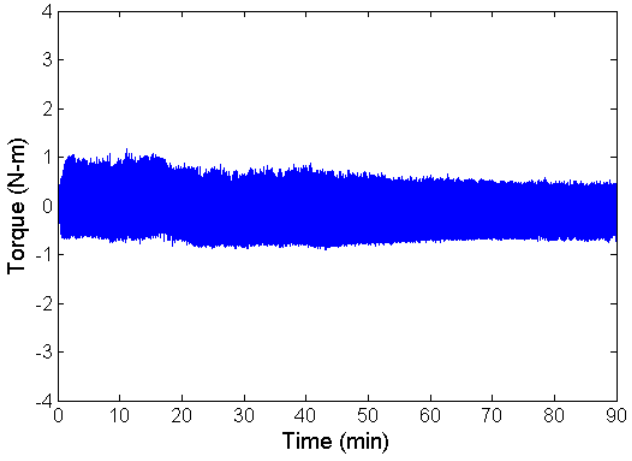

Figure C.26: Sample 30: 50 N, with sand

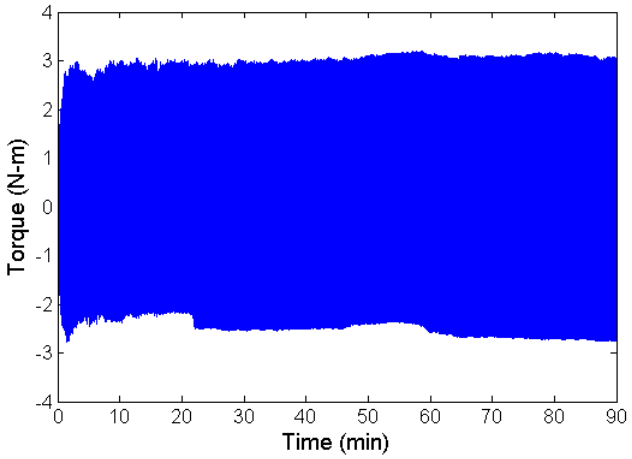

Figure C.27: Sample 31: 250 N, no sand

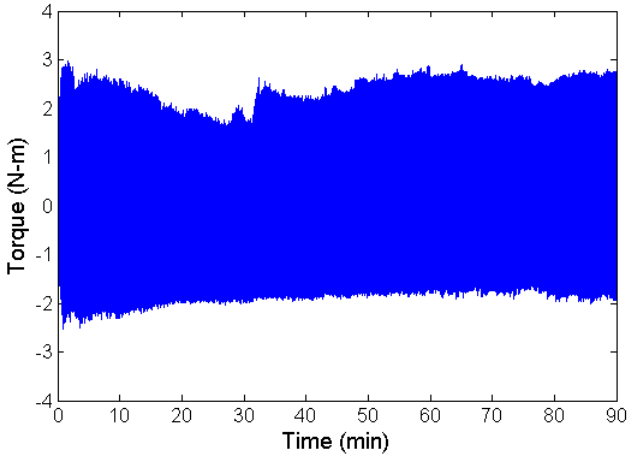

Figure C.28: Sample 32: 200 N, with sand

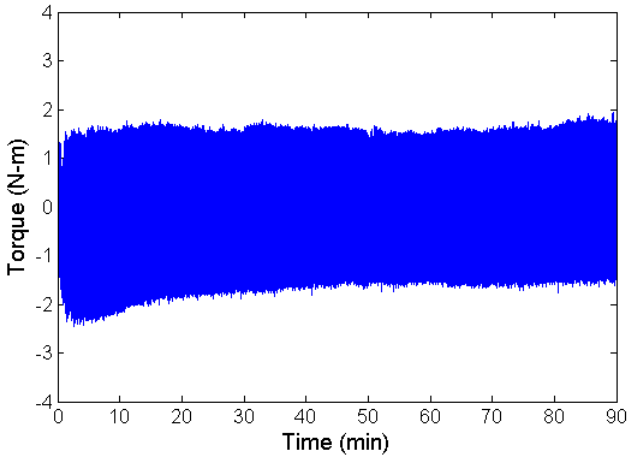

Figure C.29: Sample 33: 150 N, with sand

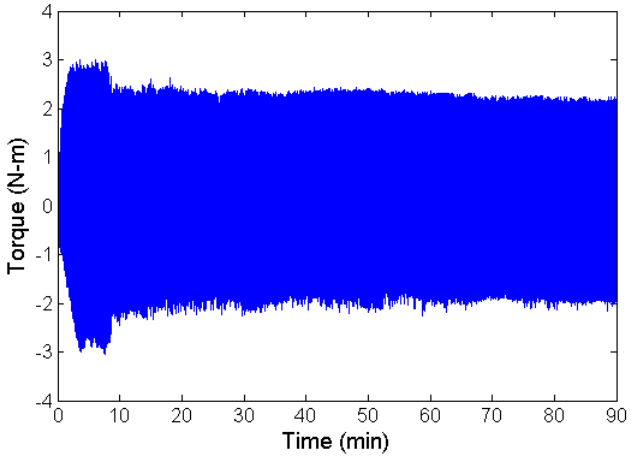

Figure C.30: Sample 34: 200 N, no sand

Appendix D

Sample Surface Profiles

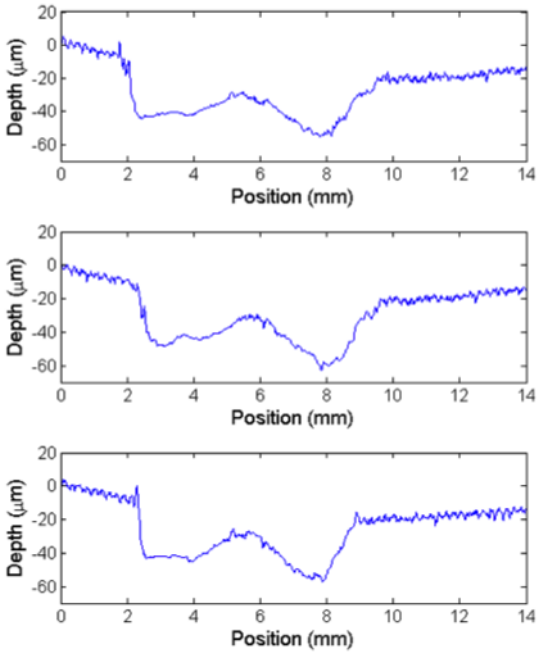

Figure D.1: Circumferential profiles from "no sand" sample

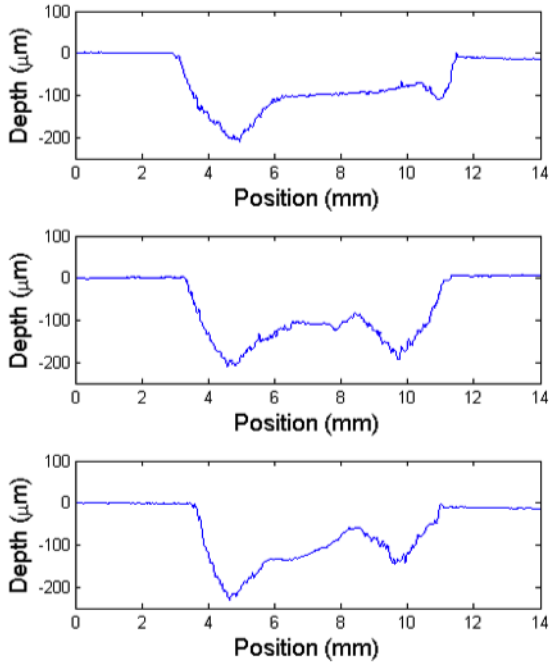

Figure D.2: Circumferential profiles from "sand after loading" sample

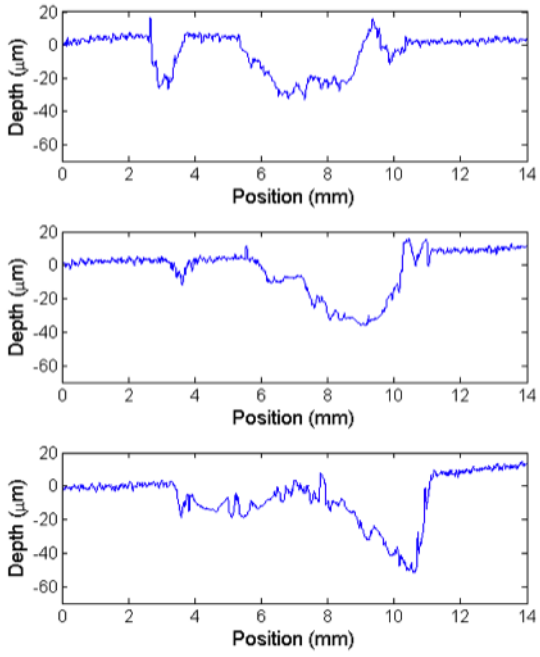

Figure D.3: Circumferential profiles from "sand before loading" sample

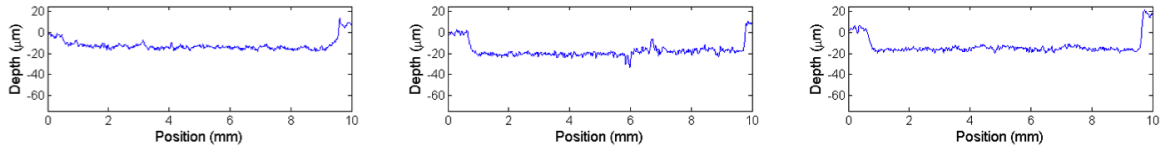

Figure D.4: Radial profiles from "no sand" sample

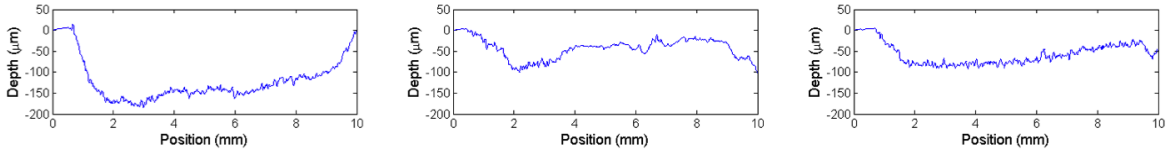

Figure D.5: Radial profiles from "sand after loading" sample

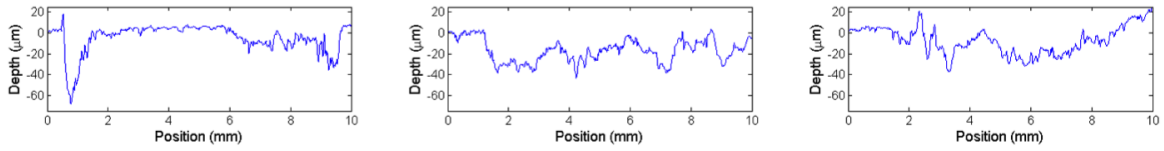

Figure D.6: Radial profiles from "sand before loading" sample